Inorg. Chem. **2008**, *47*, 10110−10126

Spectroscopic, Electrochemical, and Computational Aspects of the Charge Distribution in Ru(acac)$_2$(R-*o*-benzoquinonediimine) Complexes

Daria Kalinina, Christopher Dares, Harini Kaluarachchi, Pierre G. Potvin,* and A. B. P. Lever*

Department of Chemistry, CB124, York University, 4700 Keele Street, Toronto, Ontario, Canada M3J 1P3

Received July 31, 2008

The syntheses and properties are reported for five Ru(acac)$_2$(R-bqdi) species where acac is acetylacetonate, and R-bqdi is the non-innocent ligand *ortho*-benzoquinonediimine substituted with R = H (**1**), 4,5-dimethyl (**2**), 4-Cl (**3**), or 4-NO_2 (**4**), and *N*,*N*′-dimethylsulfonyl (**5**). Their identities and purities were confirmed by NMR, mass spectra, IR and analytical data. The large degree of metal-to-ligand π-back-donation was analyzed by spectroscopic (UV/visible, IR, Raman) and electrochemical data, supported by molecular orbital composition computations using density functional theory (DFT), with the polarizable continuum model (PCM) to mimic the presence of solvent, and prediction of electronic spectra using time-dependent DFT methods. Extended charge decomposition analysis (ECDA) and natural population analysis (NPA) both produced a detailed picture of the bonding between the non-innocent bqdi ligand and the metal center, allowing correlations to be drawn between the nature of the R substituents and the quantitative extent of π-back-donation and σ-forward donation. In conclusion, the issue of whether these species are best regarded as Ru^{II}(quinonediimine) or coupled Ru^{III}(semiquinonediiminate) species is discussed.

1. Introduction

Transition metal complexes containing quinonoid ligands are an intensively investigated area of study due to their intriguing electronic properties. The study of their ruthenium complexes has revealed a strong covalent interaction between the metal and *o*-phenylene ligands, especially *ortho*-benzoquinonediimine (bqdi) varieties,[1−8] which leads to ambiguous assignments of the formal metal oxidation states and gives rise to unique physical and chemical properties.[1,2,5,9−14] The delocalization confers organic-like behavior, with the ruthenium atom acting as an integral part of the delocalization pathway.[9] Indeed, the bqdi metallocycle ring containing the ruthenium atom is aromatic.[15−17]

We have been interested in studying the electronic structures of Ru^{II} and Ru^{III} complexes, in particular, with the bqdi ligand. The relative energies, the symmetries and overlap of valence ligand pπ and metal dπ orbitals determine the degree of their mixing, which ultimately defines the electron distribution in the system.[2,11,12,14] This includes both ligand-to-metal σ and π-donation, and d-orbital mixing with both filled π- and empty π*-levels of the ligand. This last

* To whom correspondence should be addressed. Fax: 416-736-5936. E-mail: blever@yorku.ca.

(1) Masui, H.; Lever, A. B. P.; Dodsworth, E. S. *Inorg. Chem.* **1993**, *32*, 258–267.
(2) Cunha, C. J.; Fielder, S. S.; Stynes, D. V.; Masui, H.; Auburn, P. R.; Lever, A. B. P. *Inorg. Chim. Acta* **1996**, *242*, 293–302.
(3) Metcalfe, R. A.; Dodsworth, E. S.; Fielder, S. S.; Stufkens, D. J.; Lever, A. B. P.; Pietro, W. J. *Inorg. Chem.* **1996**, *35*, 7741–7750.
(4) Metcalfe, R. A.; Lever, A. B. P. *Inorg. Chem.* **1997**, *36*, 4762–4771.
(5) Gorelsky, S. I.; Dodsworth, E. S.; Lever, A. B. P.; Vlcek, A. A. *Coord. Chem. Rev.* **1998**, *174*, 469–494.
(6) Lever, A. B. P.; Gorelsky, S. I. *Coord. Chem. Rev.* **2000**, *208*, 153–167.
(7) Sizova, O. V.; Ivanova, N. V.; Ershov, A.; Yu. Russ, J. *Gen. Chem.* **2001**, *71*, 1501–05.
(8) Venegas-Yazigi, D.; Mirza, H.; Lever, A. B. P.; Lough, A. J.; Costamagna, J.; Latorre, R. *Acta Crystallogr., Sect. C* **2000**, *C56*, e281−e282.
(9) Masui, H. Ph.D. Dissertation, York University, 1994.
(10) Lever, A. B. P.; Auburn, P. R.; Dodsworth, E. S.; Haga, M. A.; Liu, W.; Melnik, M.; Nevin, W. A. *J. Am. Chem. Soc.* **1988**, *110*, 8076–8084.
(11) Masui, H.; Lever, A. B. P.; Auburn, P. R. *Inorg. Chem.* **1991**, *30*, 2402–2410.
(12) Haga, M.-A.; Dodsworth, E. S.; Lever, A. B. P. *Inorg. Chem.* **1986**, *25*, 447–453.
(13) Gorelsky, S. I.; Lever, A. B. P.; Ebadi, M. *Coord. Chem. Rev.* **2002**, *230*, 97–105.
(14) Lever, A. B. P.; Gorelsky, S. I. *Struct. Bond. (Berlin)* **2004**, *107*, 77–114.
(15) Masui, H. *Coord. Chem. Rev.* **2001**, *219*−*221*, 957–992.
(16) Beaulac, R.; Lever, A. B. P.; Reber, C. *Eur. J. Inorg. Chem.* **2007**, 48–52.
(17) Milcic, M. K.; Ostojic, B. D.; Zaric, S. D. *Inorg. Chem.* **2007**, *46*, 7109–7114.

10.1021/ic8014496 CCC: $40.75
Published on Web 10/10/2008

process is commonly known as π-back-donation,[18] and can be estimated in terms of the Ru 4dπ contribution to the bqdi π^* LUMO. Alternatively, and more meaningfully, one may consider the free ligand bqdi π^* unoccupied orbital contributions to the occupied orbitals of the complex.

The Ru-bqdi system is of special interest because the level of π-back-donation, as qualitatively assessed by the percentage of Ru 4d character in the bqdi-localized LUMO of the complexes, can be tuned over a very wide range from less than 10% to over 30% by changing the substituent on the bqdi ligand and by varying the electron electron-richness at the ruthenium center by changing the spectator ligands. The metal electron-richness can be monitored most conveniently in terms of the ligand electrochemical parameters of these spectator ligands.[19]

A series of Ru(acac)$_2$(R-bqdi) compounds was synthesized and investigated (R = H (**1**), R = 4,5-Me$_2$ (Me$_2$) (**2**), R = 4-Cl (**3**), R = 4-NO$_2$ (**4**) and R = *N*,*N*′-di-SO$_2$Me (N-Ms$_2$) (**5**) (abbreviated below by their R group)). We present analytical, electrochemical and mass spectroscopic data to characterize these species, together with a detailed density functional theory (DFT) computational analysis (gas phase and solution phase, PCM).[20,21] This is then used to interpret the vibrational (infrared and resonance Raman) and, electronic spectra, as well as some preliminary L-edge synchrotron data. In particular, we use extended charge decomposition analysis (ECDA) and natural population analysis (NPA) to gain a better understanding of the chemical bonding in terms of symmetry and the nature of electronic interactions.[22]

These complexes are usually regarded to be complexes containing ruthenium(II) bound to the neutral quinonoid ligand.[23] Wieghardt et al. however dispute this assessment and prefer to regard them as spin-coupled ruthenium(III) complexes of benzosemiquinonediiminate (bqsdi), primarily on the basis of their metric parameters.[24] In a detailed density functional theory analysis, Remenyi and Kaupp opted for a "superposition of Ru^{III}/L$^-$ and Ru^{II}/L states rather than for a pure Ru^{III}/L$^-$ formulation".[25] We will argue that these species are indeed best regarded as Ru^{II} complexes and treat them as such for the purposes of discussing the data. In summarizing our results, section 6, we will then explore the alternative formulation as diamagnetic, spin- coupled Ru^{III} bsqdi complexes.

2. Experimental Section

All solvents and reagents used were reagent-grade or better, and used as purchased. The commercial *o*-phenylenediamines were purified by sublimation prior to use. *N*,*N*′-Di(methanesulfonyl)-*o*-phenylenediamine (N-Ms$_2$-bqdi) was prepared according to Goss et al.[26,27] [Ru(acac)$_2$(CH$_3$CN)$_2$] was prepared by a literature method.[28] The H-bqdi species complex has been previously reported.[23]

2.1. Physical Measurements. Electronic spectra were obtained on a Hewlett-Packard HP 8452A diode array spectrometer. Fourier Transform infrared (FT-IR) data were obtained using a Genesis II spectrometer with samples prepared as KBr pellets. Nuclear magnetic resonance (NMR) spectra were recorded on Bruker AM300 NMR spectrometers. For electrochemistry, Princeton Applied Research model 173 instrumentation was used along with a computer-controlled Cypress System (N-Software version 5.5). Cyclic voltammograms were obtained at a glassy carbon working electrode and a graphite counter electrode in 0.1 M tetrabutylammonium hexafluorophosphate (TBAPF$_6$) solutions in either dry acetonitrile or dimethylformamide. The reference electrode was an AgCl/Ag wire. Potentials were referenced internally to the ferrocenium/ferrocene couple (E(Fc$^+$/Fc) = 0.64 V vs NHE in CH$_3$CN).[29] Waves were deemed to be reversible if the peak cathodic current (i_c) equaled the peak anodic current (i_a), and diffusion-limited if plots of i_c vs $v^{1/2}$, where v is the scan rate, were linear. Mass spectrometry data were obtained using a Voyager-DE STR (BioSpectrometry workstation) mass spectrometer.

2.2. Computations. Geometry-optimized structures were obtained using Gaussian 03 (G03W C.02 (v6.0)) employing density functional theory (DFT) calculations, using the hybrid B3LYP exchange-correlation functional and the LANL2DZ basis set with spin-restricted wave functions for closed-shell species and spin-unrestricted wave functions for open-shell species.[30−34] Solvent (acetonitrile) was included using the polarized continuum model (PCM). A tight convergence (10^{-8} au) was used for all DFT calculations. Vibrational frequency calculations were performed on all optimized complexes to verify that an energy minimum had been attained. The wave functions were also checked for stability. All the ground states are spin singlets, but the corresponding spin triplets were also calculated to ensure that they were excited states. The energies of the predicted electronic transitions were obtained via the time-dependent DFT (TD-DFT) method.[35−37] The absorption profiles of the complexes were calculated using the SWIZARD program.[38] Extended charge decomposition analysis (ECDA) used the AOMIX-CDA program.[39] A natural population analysis (G03W) was also carried out.

(18) Chatt, J.; Duncanson, L. A. *J. Chem. Soc.* **1953**, 2939–2947.
(19) Lever, A. B. P. *Inorg. Chem.* **1990**, *29*, 1271–1285.
(20) Noodleman, L.; Lovell, T.; Han, W. G.; Liu, T.; Torres, R. A. In *Compr. Coord. Chem. II*; McCleverty, J. A., Meyer, T. J., Eds.; Elsevier: Oxford, 2003; pp 491−510.
(21) Bickelhaupt, F. M.; Baerends, E. J. In *Reviews in Computational Chemical*; Lipkowitz, K. B., Boy, D. B., Eds.; VCH Publishers: New York, 2000; Vol. *15*; pp 1−86.
(22) Gorelsky, S. I.; Ghosh, S.; Solomon, E. I. *J. Am. Chem. Soc.* **2006**, *128*, 278–290.
(23) Mitra, K. N.; Choudhury, S.; Castiñeiras, A.; Goswami, S. *J. Chem. Soc.; Dalton Trans.* **1998**, 2901–2906.
(24) Bill, E.; Bothe, E.; Chaudhuri, P.; Chlopek, K.; Herebian, D.; Kokatam, S.; Ray, K.; Weyhermüller, T.; Neese, F.; Wieghardt, K. *Chem. Eur. J.* **2005**, *11*, 204–224.
(25) Remenyi, C.; Kaupp, M. *J. Am. Chem. Soc.* **2005**, *127*, 11399–11413.
(26) Goss, E.; Grudzinski, S. *Pol. J. Chem.* **1990**, *64*, 799–804.
(27) Hieber, W.; Schnackig, A. *Z. Anor. Allgem. Chem.* **1936**, *226*, 209–221.
(28) Gupta, A. K.; Poddar, R. K. *Indian J. Chem.* **1999**, *38*, 228–231.
(29) Connelly, N. G.; Geiger, W. E. *Chem. Rev.* **1996**, *96*, 877–910.
(30) Frisch, M. J., et al. Gaussian, Inc.: Wallingford, CT, 2004.
(31) Becke, A. D. *J. Chem. Phys.* **1993**, *98*, 5648–5652.
(32) Hay, P. J.; Wadt, W. R. *J. Chem. Phys.* **1985**, *82*, 270–283.
(33) Hay, P. J.; Wadt, W. R. *J. Chem. Phys.* **1985**, *82*, 299–310.
(34) Wadt, W. R.; Hay, P. J. *J. Chem. Phys.* **1985**, *82*, 284–298.
(35) Vlcek, A.; Zalis, S. *Coord. Chem. Rev.* **2007**, *251*, 258–287.
(36) Van Gisbergen, S. J. A.; Baerends, E. J. In *Comprehen. Coord. Chem. II*; McCleverty, J. A., Meyer, T. J., Eds.; Elsevier: Oxford, 2003; pp 511−517.
(37) Grimme, S. *Rev. Comput. Chem.* **2004**, *20*, 153–218.
(38) Gorelsky, S. I. *SWizard program*, CCRI; University of Ottawa: Ottawa, Canada, 2008http://www.sg-chem.net/.
(39) Gorelsky, S. I. *AOMix: Program for Molecular Orbital Analysis*; University of Ottawa, 2007, http://www.sg-chem.net/.

2.3. Ru(acac)$_2$(bqdi) (1). A new synthetic route was developed for this known compound.[23] To a solution of [Ru(acac)$_2$(CH$_3$CN)$_2$] (0.15 g, 0.395 mmol) in absolute ethanol EtOH (30 mL), freshly sublimed 1,2-diaminobenzene (*o*-phenylenediamine) (0.043 g, 1 equiv) was added.[40] A deep red solution was obtained by heating the reaction mixture to reflux under air for ~2 h with constant stirring. The reaction mixture was then concentrated to ~2 mL, whence the desired product precipitated. After filtration and rinsing with absolute ethanol, EtOH and ether, the black precipitate was dried in vacuo. Yield 44%. ^{1}H NMR (CDCl$_3$) and IR data agree with those previously reported by Mitra et al.[23] ^{13}C NMR (CDCl$_3$): δ 26.2, 27.5, 100.0, 120.4, 115.8, 168.1, 188.8, 190.8 ppm. IR (KBr pellet, ν in cm^{-1}): 3234 (s, N−H str), 1265 (s, N−H bend), 1577 (s, C−N str), 619 (s, Ru−N$_{bqdi}$ str). LDI-MS: *m*/*z* [%] 405 [100, M], 242.[53]

2.4. Ru(acac)$_2$(4,5-(CH$_3$)$_2$-bqdi)) (2). Using the same procedure as for (**1**), but using 1,2-diamino-4,5-dimethylbenzene, a black solid was obtained with a yield of 51%. ^{1}H NMR (CD$_3$CN): δ 10.78 (2H, s), 7.13 (2H, m), 5.45 (2H, m) 2.30 (6H, s), 2.26 (6H, s) 1.68 (6H, s) ppm. ^{13}C NMR (CDCl$_3$): δ 19.9, 26.4, 27.5, 99.9, 131.3, 117.5, 167.6, 188.5, 190.1 ppm. IR (KBr pellet, ν in cm^{-1}): 2966 (s, N−H str), 1265 (s, N−H bend), 1577 (s, C−N str), 619 (s, Ru−N$_{bqdi}$ str). LDI-MS: *m*/*z* [%] 434 [100, M], Anal. Calcd for C$_{18}$H$_{25}$N$_2$O$_4$Ru: C, 49.9; H, 5.6; N, 6.5%. Found: C, 49.6; H, 5.8; N, 6.3%.

2.5. Ru(acac)$_2$(4-Cl-bqdi) (3). Using the same procedure as for (**1**), but using 1,2-diamino-4-chlorobenzene, a bright red solid was obtained with a yield of 50%. ^{1}H NMR (CDCl$_3$): δ 10.70 (H, s), 10.20 (H, s), 7. Thirty (2H, s), 7.20 (2H, d), 6.80 (2H, m), 5.45 (2H, s), 2.40 (6H, 2s), 1.80 (6H, s) ppm. ^{13}C NMR (CDCl$_3$): δ 26.3, 27.7, 100.5, 115.9, 117.1, 119.6, 127.7, 164.7, 165.4, 188.6, 190.9 ppm. IR (KBr pellet, ν in cm^{-1}): 3212 (s, N−H str), 1265 (s, N−H bend), 1577 (s, C−N str), 619 (s, Ru−N$_{bqdi}$ str). LDI -MS: *m*/*z* [%] 739 [100, 2M-Clbqdi], 440 [22, M]. Anal. Calcd for C$_{16}$H$_{19}$Cl$_1$N$_2$O$_4$Ru: C, 43.5; H, 4.6; N, 6.3%. Found: C, 43.78; H, 4.74; N, 6.13%.

2.6. Ru(acac)$_2$(4-NO$_2$-bqdi) (4). Using the same procedure as for (**1**), but using 1,2-diamino-4-nitrobenzene, a dark red solid was obtained (yield 40%). ^{1}H NMR (CDCl$_3$): δ 11.50 (H, s), 10.00 (H, s), 8.1 (H, s), 7.6 (2H, m), 7.4 (2H, m), 5.60 (2H, 2s), 2.50 (6H, s), 1.90 (6H, s) ppm. ^{13}C NMR (CDCl$_3$): δ 26.0, 26.1, 27.5, 100.2, 100.5, 110.8, 113.9, 116.3, 135.4, 161.9, 167.9, 189.0, 189.7, 192.2, 192.8 ppm. IR (KBr pellet, ν in cm^{-1}): 3305 (s, N−H str), 1261 (s, N−H bend), 1577 (s, C−N str), 619 (s, Ru−N$_{bqdi}$ str). LDI -MS: *m*/*z* [%] 749, [68, 2M-NO$_2$bqdi], 451 [100, M], 242.[58] Anal. Calcd for C$_{16}$H$_{19}$N$_3$O$_6$Ru: C, 42.5; H, 4.30; N, 9.30%. Found: C, 42.71; H, 4.41; N, 9.30%.

2.7. Ru^{II}(acac)$_2$((SO$_2$CH$_3$)$_2$-bqdi) (5). Reaction was carried out as before, but using *N*,*N*′-di(methanesulfonyl)-1,2-diaminobenzene.[26] The crude product was purified by chromatography using silica and CHCl$_3$ as an eluting solvent yielding two bands (deep red and purple). The deep red band material is the mono-N-methanesulfonylbenzoquinonediimine ruthenium complex, not discussed here. The purple band (40% yield) was found to be the desired *N*,*N*′-dimethanesulfonylbenzoquinonediimine (N-Ms$_2$) ruthenium complex. The final product was obtained with a yield of ca. 40%. ^{1}H NMR (CDCl$_3$): 7.63 (H, q), 5.29 (2H, m), 5.09 (2H, s), 3.66 (2H, s), 2.42 (6H, s), 1.84 (6H, s) ppm. LDI -MS: *m*/*z* 562, [30,M], 242.[100] Anal. Calcd for C$_{18}$H$_{23}$S$_2$N$_2$O$_8$Ru: C, 38.5; H, 4.3; N, 5.0%. Found: C, 38.8; H, 4.3; N, 5.1%.

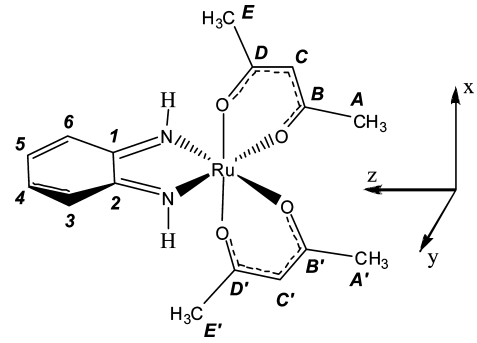

Figure 1. Generalized structure of the Ru(acac)$_2$(R-bqdi) complexes.

3. Results and Discussion

3.1. Synthesis and Identification. In an improved synthesis, Ru(acac)$_2$(bqdi) (**1**) was obtained in 44% yield from Ru(acac)$_2$(CH$_3$CN)$_2$, with product ^{1}H NMR and IR spectra consistent with those reported previously.[23] This method was also used to make the four substituted derivatives in 40−51% yields. The NMR and mass spectra were consistent with their putative structures (Figure 1). An X-ray structure of the H-bqdi species has been published.[23] ^{13}C NMR peak assignments were made using a combination of COSY, HMBC, and HSQC techniques, as well as by comparison with previous analogous compounds.

The ^{1}H NMR peaks from the imine protons appeared as broad singlets in the 10−12 ppm region. The aromatic ring protons gave rise to the expected patterns; in the unsubstituted case, this was an AA′BB′ system typical of an *o*-disubstituted benzene.[41] The methine protons of the acac ligands had chemical shifts near 5.5 ppm; this appeared as a broad singlet for the chloro-substituted complex, but appeared as a closely spaced pair of singlets in the unsymmetrical nitro-substituted case, shifted to 5.6 ppm presumably due to the stronger electron withdrawal. The acac CH$_3$ groups invariably gave rise to two signals, one in the 2.26−2.50 ppm range, the other in the 1.68−1.90 ppm range, even though four were expected with the unsymmetrical cases. Similarly, the corresponding ^{13}CH$_3$ signals also appeared as two peaks differing by 0.75−1.5 ppm. As well, pairs of ^{13}C═O signals were observed with 0.07−3.8 ppm separations. The chemical shifts of these signals and those from the methine protons, and the separations between them, roughly followed the order NO$_2$ > Cl > H > Me$_2$ > N-Ms$_2$ for the R-substituent, in accord with the donating or accepting properties of the substituent.[42] We attribute these signal separations to ring currents generated by bqdi-Ru metallocycles. Figure 1 illustrates how the axial acac CH$_3$ groups and the attached carbonyl carbons lie in the putative shielding cone above and below the N−Ru−N plane, whereas their equatorial partners, though distant, lie in the deshielding regions. NMR has previously been used to determine the presence, relative strengths, and effects of ring currents in organic aromatic materials, as well as metallocycles.[9,17] The effects of ring currents have been observed in homoleptic

(40) Gupta, A. K.; Poddar, R. K. *Indian J. Chem., Sect. A* **1999**, *38A*, 1228–1231.

(41) Werner, B. *Nuclear Magnetic Resonance Spectra and Chemical Structure*; Academic Press: New York, 1987.

(42) Hansch, C.; Leo, A.; Taft, R. W. *Chem. Rev.* **1991**, *91*, 165–195.

Ru terpyridine complexes, for example, where the protons closest to the Ru center on one ligand are shifted upfield via a through-space effect involving the ring current originating in the perpendicular ligand.[43] In the present case, the chemical shift differences are evidence of ring currents in Ru-bqdi metallocycles, which are only possible if the system has a high degree of delocalization of the Ru electron density over the bqdi ligand and if the metallocycle is flat, which is supported by the DFT results (vide infra). The exception to this trend is the R = N-Ms$_2$ species (**5**), which exhibits the smallest ring-current effect even though this species carries the most electron-poor substituent. The double signals observed in the ^{13}C NMR spectrum of the N-Ms species suggests that it does not possess C_2 symmetry, but has C_1 symmetry (there are several possible geometric isomers), making all chemical shifts slightly different for each atom. This lowering of symmetry and weakened NMR ring-current could be the result of the Ru−N metallocycle plane not being quite coplanar with the bqdi plane, which is in agreement with a DFT geometry-optimized structure, as discussed later.

The LDI-MALDI mass spectra of these species all yielded a parent peak at the appropriate *m/z* value. Interestingly, most of the species additionally exhibited a higher-mass peak corresponding to a dimer with loss of one R-bqdi. These two peaks were generally the most prominent in the mass spectra.

3.2. Electrochemical Data. Cyclic voltammetry was performed on all five complexes (Figure 2 and Supporting Information, Figure S-4). The waves were assigned by comparison with those of analogous compounds, and through the use of ligand electrochemical parameter theory.[19]

The behavior of all five compounds was very similar, each with two reversible processes within the +1 to −1 V range; an oxidation in the +0.4 V to +0.9 V range (all potentials vs NHE) believed to generate Ru^{III}-bqdi species[1,9,11,23,44−54] and a reduction process, ($E_{1/2}$(Redn),[55] Table 1) between 0.29 and −1.1 V. The relationships between the peak current and the scan rates and differential pulse voltammetry confirmed that each wave was a one-electron process under diffusion control. The acac ligand is not redox-active within the solvent window (±2.0 V). The extraordinarily large variation in the $E_{1/2}$(Redn) potential (ca. 0.80 V) for such a narrow group of complexes is noteworthy and we return to this below. The ligand reduction potentials also depend upon the Hammett parameter of the R-substituent, shifting to more positive potentials as the electron-withdrawing ability of the substituent increases.

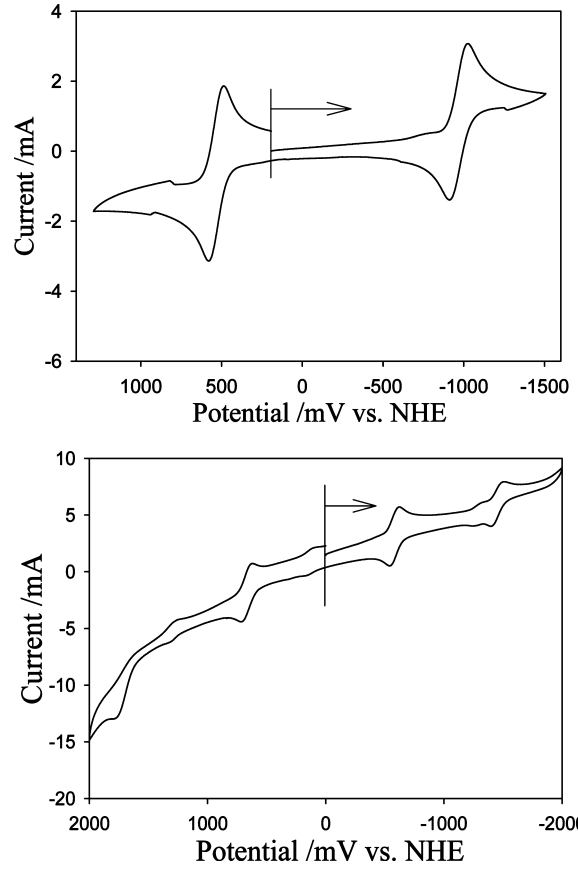

Figure 2. Cyclic voltammograms of (upper) **1** in DMF (with no other features out to ±2.0 V) and (lower) **4** in CH_3CN, both at 2×10^{-3} M and 100 mV s^{-1} in the presence of 0.1 M $TBAPF_6$. Additional very weak waves near −1100, +100 and +1200 mV are from trace impurities that were difficult to remove.

Table 1. Comparison of Electrochemical Potentials (Acetonitrile/0.1 M TBAP/ 100 mV s^{-1}) and E_L(R-bqdi) Values of the [Ru(acac)$_2$(R-bqdi)] complexes (in V vs NHE)

#	complex	$E_{1/2}$ /V vs NHE Ru$^{III/II}$	$E_{1/2}$ /V vs NHE Redn[55]	E_L(R-bqdi)
1	Ru(acac)$_2$(bqdi)	0.53	−0.96	0.42$_5$
2	Ru(acac)$_2$(4,5-(CH$_3$)$_2$-bqdi)	0.48	−1.05	0.40
3	Ru(acac)$_2$(Cl-bqdi)	0.65	−0.80	0.49
4	Ru(acac)$_2$(NO$_2$-bqdi)	0.84	−0.41	0.58
5	Ru(acac)$_2$((N-SO$_2$Me$_2$)$_2$-bqdi)	1.18	0.29	0.75

Table 1 also reports the computed E_L values for the bqdi ligands, derived from the Ru$^{III/II}$ couples using ligand electrochemical parameter theory[19,56−58] and the known E_L(acac) value of −0.08 V. The E_L(R-bqdi) values here range

(43) Luo, Y.; Potvin, P. G.; Tse, Y.-H.; Lever, A. B. P. *Inorg. Chem.* **1996**, *35*, 5445–5452.
(44) Venegas-Yazigi, D. Ph.D. Thesis, University de Chile, 2001.
(45) Venegas-Yazigi, D.; Campos-Vallette, M.; Lever, A. B. P.; Costamagna, J.; Latorre, R. O.; Hernandez, G. W. *J. Chilean Chem. Soc.* **2003**, *48*, 79–83.
(46) Venegas-Yazigi, D.; Costamagna, J.; Latorre, R.; Lever, A. B. P. In 213th ACS National Meeting San Francisco, 1997.
(47) Masui, H.; Lever, A. B. P. *Inorg. Chem.* **1993**, *32*, 2199–2201.
(48) Mitra, K. N.; Majumdar, P.; Peng, S.-M.; Castiñeiras, A.; Goswami, S. *Chem. Commun.* **1997**, 1267–1268.
(49) Mitra, K. N.; Goswami, S.; Peng, S.-M. *Chem. Commun.* **1998**, 1685–1686.
(50) Rusanova, J.; Rusanov, E.; Gorelsky, S. I.; Christendat, D.; Popescu, R.; Farah, A. A.; Beaulac, R.; Reber, C.; Lever, A. B. P. *Inorg. Chem.* **2006**, *45*, 6246–6262.
(51) Bard, A. J.; Faulkner, L. R. *Electrochemical Methods: Fundamentals and Applications*; 2nd ed.; John Wiley & Sons, Inc.: New York, 2001.
(52) Belser, P.; Zelewsky, A. v.; Zehnder, M. *Inorg. Chem.* **1981**, *20*, 3098–3103.
(53) Haga, M.-A.; Dodsworth, E. S.; Lever, A. B. P.; Boone, S. R.; Pierpont, C. G. *J. Am. Chem. Soc.* **1986**, *108*, 7413–7414.
(54) Mederos, A.; Dominguez, S.; Hernandez-Molina, R.; Sanchiz, J.; Brito, F. *Coord. Chem. Rev.* **1999**, *193−195*, 913–939.
(55) This reduction is now associated with an internal redox process to form a Ru^{III} complex of the double reduced diamidobenzene(2-) ligand. See further comment below.
(56) Lever, A. B. P. *Comprehen. Coord. Chem. II*; McCleverty, J. A., Meyer, T. J., Eds.; Elsevier: Oxford, 2003; Vol. *2*, pp 251−268.
(57) Lever, A. B. P.; Dodsworth, E. S. *Inorganic Electronic Structure and Spectroscopy*; John Wiley: Boston, 2004; Vol. *2*., pp 227−287.

from 0.41 to 0.75 V (vs NHE), increasing, generally, as the π-accepting nature of the R-bqdi ligand increases,[9,50,59] as monitored by the Ru(4d) character in the LUMOs; indeed there is a linear relationship between the Hammett parameter, $\Sigma\sigma_P$, and the E_L value for substituted ligands.[47] Usually, the second reduction couple occurs at too negative a potential to be observed, but the nitro group is sufficiently electron-withdrawing that this process is shifted within the measurable range in the case of 4.

4. Computation and Electronic Structure

4.1. Molecular Orbital Description. We have previously discussed, in some depth, the electronic structures of *o*-benzoquinonediimine complexes of ruthenium.[1,4−6,13,14,16,50,60−67] Both INDO and DFT computational methods were used previously (with similar results) to explore the extent of covalent mixing between the metal and the *o*-benzoquinonediimine ligand, and especially the extensive degree of π-back-donation prevalent in these complexes. In this study, we use DFT exclusively and primarily consider solution solution-phase calculations using the PCM;[20,68] these provide a slightly better fit to the electronic spectra than if the gas-phase optimizations are used. The discussion will be based on the more commonly assumed Ru^{II} bqdi formulation, but we will return in Section 6 to the problem as to whether these species are better regarded as spin-coupled Ru^{III} complexes of *o*-benzosemiquinonediiminate (bsqdi).[25] For ease of discussion, we define [Ru(acac)$_2$] as fragment 1 and R-bqdi as fragment 2.

To discuss the interactions of the metal orbitals with the chelated ligands, a coordinate system is defined where the bqdi ligand lies in the *yz* plane with the *z*-axis bisecting the bqdi ligand (Figure 1). The *x*-axis is therefore perpendicular to the bqdi ligand. In this coordinate system, the three d(t_{2g}) orbitals in O_h are then described as dδ (d_{xy}), dπ (d_{xz}) and dσ ($d_{y^2-z^2}$) with respect to the bqdi plane, while the two remaining d(e_g) orbitals in O_h, d_{yz}, d_{x^2} are then both described as dσ*.[69,70] We are, in effect, treating the bqdi fragment as belonging to the C_{2v} point group. This is an excellent approximation for the [Ru(acac)$_2$] parent (R = H) and dimethyl species (R = Me_2) where the complexes belong to the C_2 group. With the other substitutions, R = Cl, NO_2, N-Ms_2, the t_{2g} set can still be recognized visually to be approximately dσ, dδ, and dπ with respect to R-bqdi, despite deviation from C_2 symmetry. The charge redistribution which occurs on binding this [Ru(acac)$_2$] fragment to the R-bqdi fragment can best be addressed by viewing these components separately, and then observing the changes which occur when they are bound to each other.

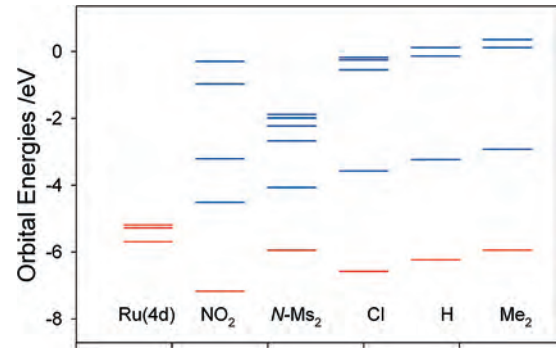

Figure 3. Comparison of DFT (PCM, acetonitrile) calculated frontier orbital energies for the individual fragments: Ru(acac)$_2$ 4d (t_{2g}) orbitals (red) and the HOMO (red), LUMO and higher virtual orbitals (blue) of the ligand (R-bqdi). The geometry of the free ligands is that appropriate to the complex being formed with the [Ru(acac)$_2$] fragment.

For R = H, Cl or, Me, the LUMO and LUMO+1 of the R-bqdi *free ligand* are π* orbitals of appropriate symmetry (b in C_2) to couple to the Ru 4dπ orbital, while LUMO+2 has δ* symmetry (a in C_2) and can couple with 4dδ. With R = NO_2, the LUMO+2 is also π* and LUMO+3 is δ*. For R = *N*-Ms, the LUMO is π* but then there are two σ* orbitals that lie lower than the next π* (LUMO+3) and δ* (LUMO+4) orbitals. Figure 3 compares the energies of the frontier orbitals of the complexes of the two fragments. The HOMO and LUMO of R-bqdi become progressively more stable with an increasing acceptor character of the substituent, while the HOMO−LUMO gap remains roughly constant.

In assembling the fragments, we can anticipate that the greatest covalency may be found where there is the best energy match between Ru 4d and ligand frontier orbitals, probably with R = *N*-Ms_2 and NO_2. Turning to the complexes, good agreement has been found between experimental bond distances from analogous X-ray structures, and the (gas- or solution-phase) optimized geometries of the complexes obtained using the B3LYP exchange-correlation functional, with the LANL2DZ basis set (see Supporting Information Table S1, and *xyz* coordinates in Tables S15−19, and discussion in Section 6 below).[71] All the species studied showed a pseudo-octahedral geometry about Ru. The unsubstituted, dimethyl-substituted and methanesulfonyl complexes potentially can belong to the C_2 point group, while the other substituted bqdi species belong to the C_1 point group. In fact the best (lowest energy) solutions for the unsubstituted and dimethyl-substituted species did belong to the C_2, group. A C_1 conformation of the R = *N*-Ms_2 species

(58) Dodsworth, E. S.; Vlcek, A. A.; Lever, A. B. P. *Inorg. Chem.* **1994**, *33*, 1045–1049.
(59) Dodsworth, E. S.; Lever, A. B. P. *Coord. Chem. Rev.* **1990**, *97*, 271–284.
(60) Lever, A. B. P.; Masui, H.; Metcalfe, R. A.; Stufkens, D. J.; Dodsworth, E. S.; Auburn, P. R. *Coord. Chem. Rev.* **1993**, *125*, 317–332.
(61) Da Cunha, C. J.; Fielder, S. S.; Stynes, D. V.; Masui, H.; Auburn, P. R.; Lever, A. B. P. *Inorg. Chim. Acta* **1996**, *242*, 293–302.
(62) Ebadi, M.; Lever, A. B. P. *Inorg. Chem.* **1999**, *38*, 467–474.
(63) Metcalfe, R. A.; Vasconcellos, L. C. G.; Mirza, H.; Franco, D. W.; Lever, A. B. P. *J. Chem. Soc.; Dalton Trans.* **1999**, 2653–2667.
(64) Da Cunha, C. J.; Dodsworth, E. S.; Monteiro, M. A.; Lever, A. B. P. *Inorg. Chem.* **1999**, *38*, 5399–5409.
(65) Masui, H.; Freda, A. L.; Zerner, M. C.; Lever, A. B. P. *Inorg. Chem.* **2000**, *39*, 141–152.
(66) Gorelsky, S. I.; Lever, A. B. P. *J. Organomet. Chem.* **2001**, *635*, 187–196.
(67) Gorelsky, S. I.; Lever, A. B. P. *Can. J. Anal. Sci. Spectry* **2003**, *48*, 93–105.
(68) Cossi, M.; Barone, V.; Mennucci, B.; Tomasi, J. *Chem. Phys. Lett.* **1998**, *286*, 253–260.
(69) Figgis, B. N.; Hitchman, M. A. *Ligand Field Theory and Its Applications*; Wiley-Interscience: New York, 2000.
(70) Lever, A. B. P. *Inorganic Electronic Spectroscopy*; Elsevier: Amsterdam, 1984.

(71) DFT geometry-optimized structures for all complexes are included in the Supporting Information section.

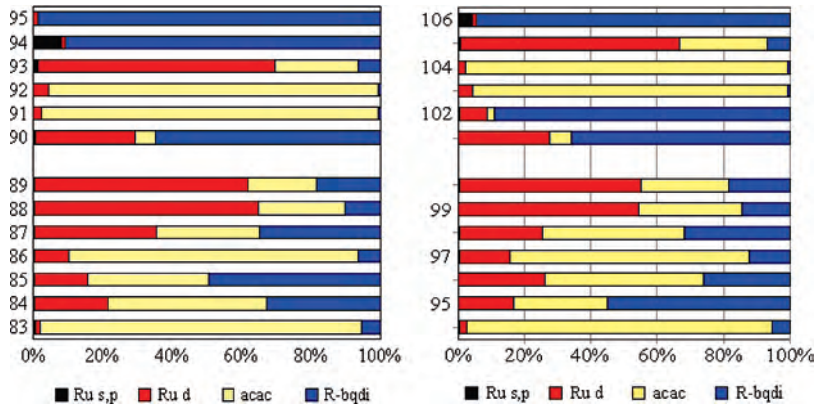

Figure 4. Percent composition of frontier orbitals of (left) Ru(acac)$_2$(bqdi) (**1**) and (right) Ru(acac)$_2$(NO$_2$-bqdi) (**4**) (B3LYP/LANL2DZ) /PCM solution phase calculation, in acetonitrile).

was of slightly lower energy, and correlated with the experimental data rather better than the C_2 isomer, and was therefore employed.

The MO compositions in terms of orbital contributions from Ru (s,p,d), acac and R-bqdi were estimated for all species.[6,14,22,39,66,67] Figure 4 shows the percent orbital compositions of the parent (R = H) and the R = NO$_2$ species (PCM, acetonitrile). Corresponding data for the other species are provided in Supporting Information Tables S-10−14.

There is clearly extensive mixing between Ru 4d orbitals and molecular orbitals of both acac and R-bqdi MOs. The HOMO, HOMO-1, and HOMO-2 are Ru 4dδ, 4dσ, and Ru 4dπ, respectively, in all the species under consideration, and it is evident that the 4dπ (HOMO-2) orbital is most heavily mixed, that is, the least pure of these orbitals which derive from the octahedral 4d(t_{2g}) set. Data for some frontier orbitals are shown in Table 2, with a more extensive set provided in Supporting Information Table S-6, Figure S-5. The LUMO of the complexes is predominantly localized on the R-bqdi ligand and has π-symmetry in all cases. It is the primary conduit for a π-covalent interaction with the metal center commonly called π-back-donation,[18] and to which we return below. This orbital has 29−32% Ru(4d) character in all complexes (Table 2, Figure 4). The LUMO+1 of the complex, for R = H, Cl or, Me$_2$ is primarily localized on acac, while for R = NO$_2$ and *N*-Ms$_2$, it is primarily localized on R-bqdi. Noteworthy are the fairly extensive contributions of 4d character to HOMO-3/4/5 which provide a conduit to couple acac and R-bqdi orbitals. HOMO-3 is especially relevant because it has the same symmetry as the LUMO and electronic transitions therefrom to the LUMO contribute significantly to the visible region spectrum. For Ru(acac)$_2$-(bqdi), HOMO-4 contains 43.5% of the π-symmetry HOMO of fragment 2 (HOF_2O (2)) while HOMO-5 (#84 in Figure 4 (left)) contains 23.4% of the π-symmetry HOF_2O. Some examples of the Kohn−Sham orbitals are shown in Figure 5.

4.2. Electronic Structure and Extent of Back-Donation. We now discuss the electronic structures, in greater depth and explore how these are influenced by the changing substitution on bqdi. Extended charge decomposition analysis

Table 2. Percent Contributions to Frontier MOs of Ru(acac)$_2$(R-bqdi) Species in Solution Phase (B3LYP/LANL2DZ, (Acetonitrile))

R-bqdi	#MO	%Ru (s,p)	%Ru(4d)	%acac	%R-bqdi
H	LUMO+1	0.0	2.3	96.9	0.7
	LUMO	0.6	28.6	6.0	64.8
	HOMO	0.4	61.4	20.1	18.2
	HOMO-1	0.1	64.8	25.2	10.0
	HOMO-2	0.4	35.2	29.8	34.6
	HOMO-3	0.3	9.9	83.2	6.5
Me_2	LUMO+1	0.0	2.5	96.7	0.8
	LUMO	0.7	27.3	5.9	66.2
	HOMO	0.4	61.7	19.1	18.8
	HOMO-1	0.1	66.0	24.2	9.8
	HOMO-2	0.4	38.1	25.9	35.6
	HOMO-3	0.3	8.0	85.8	5.8
Cl[a]	LUMO+1	0.0	2.3	97.0	0.7
	LUMO	0.5	30.1	6.3	63.1
	HOMO	0.4	60.8	21.9	16.9
	HOMO-1	0.1	63.2	26.5	10.2
	HOMO-2	0.4	31.5	32.7	35.4
	HOMO-3	0.3	10.9	80.3	8.4
NO_2	LUMO+1	0.5	8.3	2.1	89.2
	LUMO	0.1	27.7	6.4	65.8
	HOMO	0.4	54.7	26.5	18.4
	HOMO-1	0.2	54.3	31.1	14.5
	HOMO-2	0.4	25.1	42.8	31.7
	HOMO-3	0.4	15.3	72.2	12.2
N-Ms_2	LUMO+1	0.8	9.1	4.3	85.9
	LUMO	0.1	33.2	9.1	57.5
	HOMO	0.3	42.5	37.7	19.5
	HOMO-1	0.2	48.3	30.8	20.7
	HOMO-2	0.2	23.3	41.6	34.9
	HOMO-3	0.5	13.3	71.5	14.8

[a] Species is insoluble in acetonitrile. Data are reported for methanol. However, calculated data in acetonitrile are almost identical to these data.

(ECDA)[22,72,73] and natural population analyses (NPA) were used to provide both a better qualitative and quantitative understanding of the chemical bonding in these species. The resulting MO interaction diagrams (Figure 6 and Supporting Information) allow for the easy identification of the orbital interactions which would otherwise be more difficult to deconvolute.

Table 3 summarizes the data which can be derived by using this ECDA procedure and correlates the results with experimental data. Note that the methodology used here relies

(72) Dapprich, S.; Frenking, G. *J. Phys. Chem.* **1995**, *99*, 9352–9362.
(73) Gorelsky, S. I.; Solomon, E. I. *Theor. Chem. Acc.* **2008**, *129*, 57–65.
(74) The orbital interaction diagrams generated by ECDA for all complexes are included in the supplementary information section.

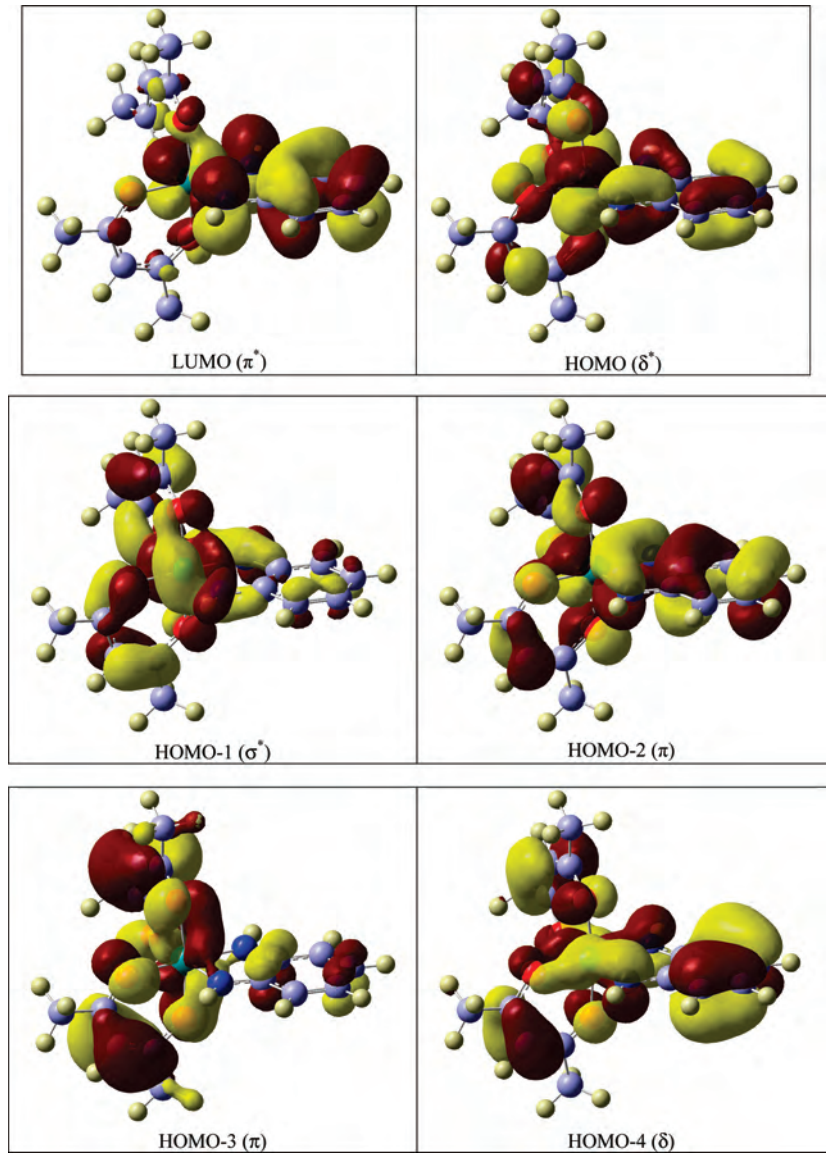

Figure 5. Kohn−Sham molecular orbital MO renderings for $Ru(acac)_2$(H-bqdi) (**1**).

on Mulliken population analysis and can be compared with the natural population analysis, NPA, discussed below (Section 4.3). As will be demonstrated, there is a good relationship between theory and experiment, providing confidence that the overall analysis is valid.

We observe the $E_{1/2}$[Redn] potentials (Table 1) to lie in the sequence (increasingly more negative):

$$N\text{-}Ms_2\text{-bqdi} > NO_2\text{-bqdi} > Cl\text{-bqdi} > H\text{-bqdi} > Me_2\text{-bqdi} \quad (1)$$

while we can extract E_L(R-bqdi) values (Table 1) from the observed $E_{1/2}$ [$Ru^{III/II}$] lying in the same sequence (eq 1). The reduction potentials and E_L(R-bqdi) are linearly related (Figure 7), as expected.[57,75] Further, as the quinone ligand becomes a better π-acceptor through substitution with electron-accepting substituents, the E_L(R-bqdi) value should increase. This is seen to be the case through a linear relationship (Figure 7) between E_L(R-bqdi) and the substituent Hammett σ_r value (Table 3) of the substituent (Figure 7), a relationship previously noted.[1,4,47,75]

As discussed in depth previously,[6,13,50,67] the extensive covalency, or π-back-donation, in these complexes is monitored qualitatively through the %Ru 4d character in the LUMO, which is a π*-orbital mostly localized on the R-bqdi ligand and is antibonding with respect to metal dπ. For these species, this percentage is ca. 27−33% (Table 3) similar to that observed with $Ru(NH_3)_2Cl_2$(bqdi) and is very significantly larger than observed in other Ru diimine species such as complexes of 2,2′-bipyridine (cf. 5−6% for %Ru 4d in the bipyridine-localized π* LUMO of $Ru(bpy)_2Cl_2$, bpy = 2,2′-bipyridine).

However, the LUMO of the complex is a virtual orbital, and it is misleading to say that electrons are back-donated to it. Thus, a more direct value for back-electron transfer can be found by assessing the contribution (mixing) of the relevant π* (and δ*) orbitals of R-bqdi (invariably the

(75) Lu, S.; Strelets, V. V.; Ryan, M. F.; Pietro, W. J.; Lever, A. B. P. *Inorg. Chem.* **1996**, *35*, 1013–1023.

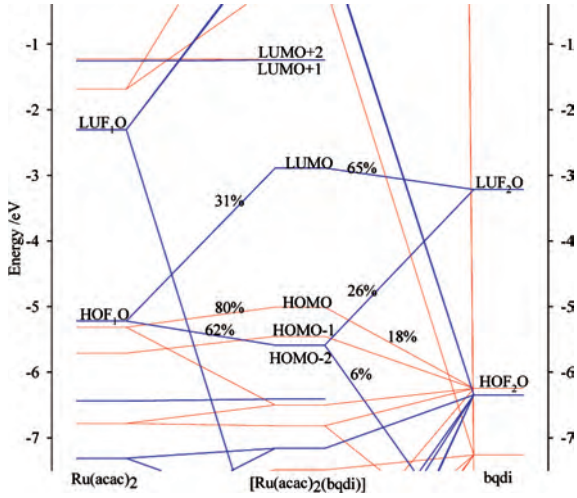

Figure 6. Orbital interaction diagram, generated by ECDA,[74] for the DFT-optimized structure of Ru(acac)$_2$bqdi (**1**), using the B3LYP exchange-correlation functional and the LANL2DZ basis set (PCM, acetonitrile), produced using the AOMIX-CDA program.[39] A line connects a fragment orbital (FO) to a given MO if the contribution of that FO is at least 5%. In the C_2 symmetry, the orbital assignments of a and b symmetry are individually colored. Diagrams for the other species discussed here can be found in Supporting Information.

LUMO of R-bqdi, is by far the largest contributor) to *filled* orbital(s) of the complex, on the metal center, dominantly dπ (and dδ) in the high-symmetry case. In the C_1-symmetry species, the π and δ labels are less relevant, through mixing, and σ-orbitals may also be involved. However, even in this situation, the LUMO of R-bqdi is dominant.

Then, for example, for Ru(acac)$_2$(bqdi), the bonding HOMO-2 is comprised primarily of 61.8% of the HOMO of fragment 1, designated HOF$_1$O (1) (which is mostly 4dπ) and 26.2% LUF$_2$O (2) (the LUMO of fragment 2) (also see Figure 6). Since the HOMO-2 is filled, the 26.2% LUF$_2$O (2) component provides the mechanism to back transfer 0.52 electrons to R-bqdi. There are other filled orbitals of appropriate symmetry into which LUF$_2$O (2) is mixed but to a much lesser degree. When these are all summed, the total π-back electron transfer is 0.64 electrons. This is the dominant π-back electron transfer process. In addition, there will be higher-lying virtual orbitals on R-bqdi (especially in the C_1 species) which may be mixed with filled orbitals of the complex, providing an additional path for back-electron transfer. The total amount of charge back-donated from fragment 1 to fragment 2 (R-bqdi) is given by the total % contribution (mixing) of *unoccupied* orbitals of fragment 2 to *occupied* orbitals of the complex. For Ru(acac)$_2$(bqdi) (**1**) this is 0.76 electrons (Table 3). Thus, in this case, these higher-lying orbitals provide a path for an additional 0.12 e transfer to R-bqdi above that provided by the mixing of LUF$_2$O (2) (0.76 − 0.64)e. For comparison purposes, we note in passing that the charge transferred to the π^* LUMO of Ru(PPh$_3$)$_2$Cl$_2$(glyoxalbis(*N*-phenyl)osazone) (also a di-imine fragment) was reported to be 0.32 electrons (cf. 0.52 above).[76] For the lower-symmetry nitro species (**4**), 0.76 electrons are back-donated via mixing of the LUF$_2$O (2) into filled orbitals of the complex, but the LUF$_2$O+1 (2) and LUF$_2$O+2 (2) are also of π-character and their mixing contributes 0.11 and 0.04 electrons, respectively, to π-back-electron transfer. Higher lying virtual orbitals also contribute to filled MOs to a total of 0.97 au (Table 3).

The R-bqdi ligand donates charge to fragment 1 primarily by a σ-mechanism formally using (in valence bond terms) the lone pairs on NH, that is, filled orbitals on fragment 2 primarily localized on the coordinating nitrogen atoms mix with appropriate-symmetry empty orbitals on fragment 1. The total amount of charge donated to fragment 1 from fragment 2 is given by the total % contribution (mixing) of *unoccupied* orbitals of fragment 1 to *occupied* orbitals of the complex. For Ru(acac)$_2$(bqdi) (**1**), this is 0.72 electrons (Table 3).

Then the overall net charge residing on the R-bqdi ligand in the complex, can be derived from the difference between the net donation of charge from the ligand to the metal by σ- and π-mechanisms (Table 3) and the net π-back-donation from metal to ligand. It will not exactly equal this difference because of polarization effects (Table 3) caused by the interaction of the two fragments (where the presence of one fragment influences the charge distribution between occupied and unoccupied orbitals in the other fragment); these are expected to be very small in systems with extensive delocalization, as is the case here. This has been discussed, in depth, by Gorelsky et al. elsewhere.[22,73] The net charge on R-bqdi (Table 3) varies from +0.02 in R = Me$_2$, to −0.49 au in R = N-Ms$_2$, and falls in the same sequence as the reduction potentials (eq 1), with the greatest negative charge on the *N*-Ms$_2$ system. The ligand itself is formally neutral (within the Ru^{II}-quinone formulation) and, in the usual M-L bonding framework, one expects that σ-donation in the formation of σ-bonds will normally lead to a net positive charge residing on a ligand which is initially neutral. Obviously, here, π-back-donation conveys more charge back to the ligand than is conveyed to the metal by σ-bond formation (and any additional π-donation) (for all except R = Me$_2$).[50]

This net charge, derived computationally, correlates admirably with observable experimental data. Thus, Figure 8 shows an outstanding linear relationship (r^2 = 0.999) between this calculated net charge residing on the R-bqdi fragment and the experimentally observed electrochemical ($E_{1/2}$([Redn]) reduction potential and a similar relationship to E_L(R-bqdi). These impressive correlations between experimental observables and a DFT predicted charge provides confidence in the significance of the theoretical analysis. The correlation with E_L(R-bqdi) may initially be unexpected since we compare five different ligands, but we have shown above that E_L(R-bqdi) linearly correlates with the Hammett value of the substituent so the changing substituent is then effectively linearly taken care of. One should reflect, however, that the redox potentials depend on the relative stability constants of the pertinent oxidized *and* reduced species and the calculation relates only to the properties of one of these components. Linearity implies that the properties of both components must behave in a linear fashion with the variable concerned. With respect to the Hammett plot, one might also

(76) Roy, A. S.; Tuononen, H. M.; Rath, S. P.; Ghosh, P. *Inorg. Chem.* **2007**, *46*, 5942–5948.

Table 3. Summary of Computed Properties of the M(acac)$_2$(R-bqdi) Species (PCM, Acetonitrile) (ECDA)

property/species	(**5**) *N*-Ms$_2$	(**4**)NO$_2$-bqdi	(**3**) Cl-bqdi	(**1**) H-bqdi	(**2**) Me$_2$-bqdi	(**8**) Zn-bqdi[a]	(**10**) Fe-bqdi[b]
Mayer Bond Order[c]	2.22	2.31	2.21	2.18	2.16	0.44	2.03
%M (d) in LUMO	33.2	27.7	30.7	28.7	27.3	0.3	22.8
% bqdi in LUMO	57.5	65.8	62.9	64.7	66.2	98.6	74.0
π-charge transfer[d,e] (a.u.)	1.07	0.97	0.81	0.76	0.73	0.04	0.57
σ,π-donation[e] (a.u.)	0.57	0.77	0.75	0.72	0.76	0.25	0.78
polarization[e] (a.u.)	−0.01	−0.01	0.002	−0.02	0.004	0.02	0.004
net charge on R-bqdi (a.u.)	−0.49	−0.19	−0.06	−0.02	+0.02	+0.19	+0.20
Mulliken charge on M	0.71	0.61	0.58	0.57	0.56	0.98	0.22
Hammett σ_p	1.44	0.78	0.23	0.00	−0.34	0	0

[a] Zn(acac)$_2$(bqdi) (**8**) (gas phase). [b] Fe(acac)$_2$(bqdi) (**10**) (gas phase). [c] Net bond order between the [Ru(acac)$_2$] and R-bqdi fragments. [d] π-electron back-donation. [e] See text for method of derivation of these data.

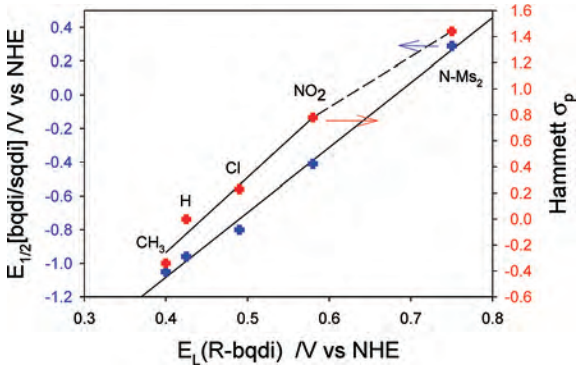

Figure 7. Plots of (left axis) $E_{1/2}$[Redn] (/V vs NHE) and (right axis) Hammett σ_p values versus E_L(R-bqdi) (/V vs NHE).

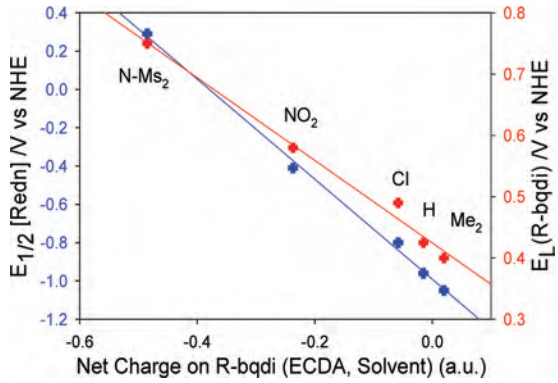

Figure 8. Plots of (blue) $E_{1/2}$[Redn] (/V vs NHE) and (red) the value of E_L(R-bqdi) (/V vs NHE) versus the net charge (ECDA) (PCM, acetonitrile) residing on the R-bqdi ligand (a.u.). The R labels are aligned with the corresponding entries.

note that the value of σ used for the *N*-Ms$_2$ is that appropriate for a C-substituent,[42] but it is evidently not far from the correct value for the *N*-substituent. The species with the largest net negative charge on bound R-bqdi, the *N*-Ms$_2$ species, is the easiest to reduce (to R-bqsdi) and the most difficult to oxidize (to Ru^{III}). The free ligand ((*N*,*N*′-SO$_2$Me)$_2$-bqdi), is the *least basic donor* and is also a good π-acceptor.

Thus, charge is significantly stabilized on the ligand, favoring reduction, and it has been removed from the metal, disfavoring oxidation to Ru^{III}. We have geometry optimized (DFT, UB3LYP/LANL2DZ, PCM acetonitrile) these one-electron reduced species and derived their energies.[77] The increased stabilization of these complexes with increasing acceptor capability of the R-bqdi ligand is displayed in Figure 9, where the reduction potential is plotted against the

(77) Kalinina, D.; Krainova, J.; Lever, A. B. P., to be submitted, 2008.

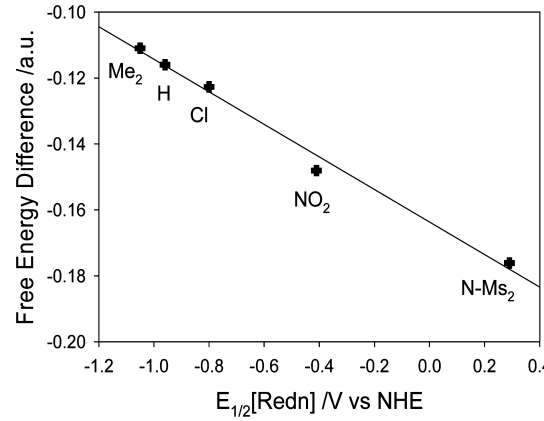

Figure 9. Plot of the experimentally observed reduction potential (V vs NHE) in acetonitrile versus the net free energy gain (PCM, acetonitrile, DFT, a.u.) upon one-electron reduction of the complex.

difference in free energy of the parent and reduced species. This is illustrative of the gain in stabilization energy of the reduced species as the R-bqdi ligand becomes a better acceptor. This correlation is impressive in that it shows a wide range of experimental reduction potentials agreeing linearly ($r^2 = 0.99$) with a theoretically computed, very small, difference between two large numbers. The stabilization energy is approximately 0.01% of the total energy.

Table 3 reveals that the *N*-Ms$_2$ species (**5**) is rather different from the ring-substituted species. Thus, despite having the highest net negative charge, the net Mayer bond order[78,79] between the [Ru(acac)$_2$] and [R-bqdi] fragments (Table 3) is lower than for R = NO$_2$, yet the %Ru 4d character in the LUMO (Table 3) is the largest. Figure 10, 11 plots Mayer bond order (col. 1) and net π-electron charge transfer versus net charge on the R-bqdi ligand. These plots are linear for the *C*-substituted species (Net charge transfer $r^2 = 0.999$; Mayer $r^2 = 0.97$, if the *N*-Ms$_2$ data are treated as outliers). The reason for this outlier behavior can be discerned from Table 3. The net charge is a difference between the net donation and net acceptor character (corrected for polarization) and all the *C*-substituted species donate essentially the same amount of charge, 0.75 e (from 38.2 ± 0.5% (Table 3) (and have roughly the same polarization contribution) and thus the linear behavior seen in Figures 79 is primarily tracking the changing π-acceptor character. The *N*-Ms$_2$ substituents make the *N*-Ms$_2$ ligand a

(78) Mayer, I. *Chem. Phys. Lett.* **1983**, *97*, 270–274.
(79) Bridgeman, A. J.; Cavigliasso, G.; Ireland, L. R.; Rothery, J. *J. Chem. Soc., Dalton Trans.* **2001**, 3556–3563.

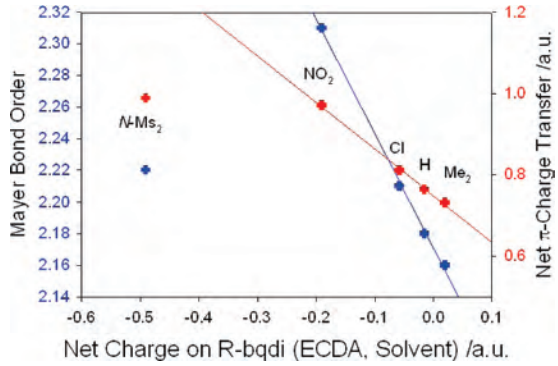

Figure 10. Plots of Mayer bond order (left, blue) and net π-electron back-donation (right, red) versus net charge on the R-bqdi ligand (a.u.) (ECDA, PCM, acetonitrile).

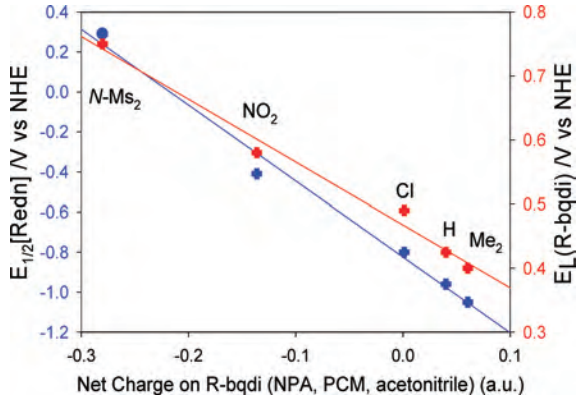

Figure 11. Plots of (blue) $E_{1/2}$[Redn] (/V vs NHE) and (red) the value of E_L(R-bqdi) (/V vs NHE) versus the net charge (NPA) (PCM, acetonitrile) residing on the R-bqdi ligand (a.u.). The R labels are aligned with the corresponding entries.

much weaker donor (0.57 e net charge donation). Thus, the much greater net charge on this ligand arises because it is a much poorer donor as well as a much better acceptor, and it shows nonlinear behavior in Figure 10. The *N*-Ms$_2$ data are not outliers in Figures 7−9 where the provenance of the net charge was largely irrelevant. As a control, we also display in Table 3 comparative data calculated for the hypothetical (3d) species Zn(acac)$_2$(bqdi) (**8**) and Fe(acac)$_2$-(bqdi) (**10**). As would be anticipated, for the Zn species there is essentially no Zn contribution to the LUMO which is close to 100% localized on the bqdi. Back-donation is also miniscule, while σ-donation shows a much weaker bond than for the Ru analogue. The Mulliken charge on Zn is close to unity and the net charge on the, definitively quinonoid, bqdi ligand is +0.19 a.u. In the Fe case, we expect that a poorer match of orbital energies between bqdi and Fe, and a more ionic bond than for Ru, would make for less π-back-donation. Indeed the net π-back-donation is significantly less (Table 3) and the net charge on bqdi is now positive.

4.3. Natural Population Analysis (NPA). An NPA calculation was carried out (Table 4)[80,81] with similar results to the ECDA analysis showing net charge on R-bqdi becoming more negative from R = Me$_2$ to NO$_2$ and then *N*-Ms$_2$. The overall negative charge is, however, somewhat smaller than that derived by the ECDA analysis. The two methods are similar but differ in the way they factor the charge. The NPA is less sensitive to the choice of basis set than is the ECDA. They correlate linearly with each other with an $r^2 = 0.99$ (exclusive of R = *N*-Ms$_2$, with this latter point, $r^2 =$ is 0.94; graph not shown). The natural charge on the Ru is ca. +1.0 au, somewhat larger than the calculated Mulliken charge and, importantly, essentially independent of the R-bqdi ligand, that is, between R= Me$_2$ and NO$_2$, *N*-Ms$_2$, the charge on Ru changes by 0.07 a.u., while that on R-bqdi changes by 0.28 a.u. Thus the steadily increasing negative charge on R-bqdi from R = Me$_2$ to R = *N*-Ms$_2$ is seen to be compensated by a significant decrease in the negative charge residing on the acac ligands, and not simply by charge transfer from Ru. The net negative charge on the coordinating nitrogen atoms is essentially constant for all the Ru^{II} bqdi species.

The geometry optimized excited-state spin triplet of species **1** (species **1*a**) is included in Table 4 to facilitate later discussion. It may be regarded as a Ru^{III} linked to benzosemiquinonediiminate with the spins on each fragment ferromagnetically coupled. Calculation reveals that the spin density is close to 1 on both the Ru^{III} and bsqdi fragments. Note that the charge on Ru in **1*a** is substantially larger than for the ground-state spin singlet, and similar to species **7** which is the one-electron oxidation product of species **1** and also assumed to contain Ru^{III}. The quinonoid fragment, in **1*a**, has increased in net charge by about 0.16 au compared to the spin singlet species and this extra charge is roughly equally provided by Ru and the acac ligands, both of which have lost about 0.1 au of charge relative to the spin singlet. This increase of 0.16 au is much smaller than seen in species **8** and **9**; however, this is understandable in that species **9** carries one net negative charge more than species **8**.

Note, in passing, that the NPA charge on the Ru^{III} in **6** (Table 4) is substantially less than in the cation (oxidized species), which more clearly contains Ru^{III}, and is indeed smaller than any of the species listed in Table 4 except for the Fe^{II} complex. The NPA charge on the bcat ligand is also less negative than on the bsqdi in the Zn species; thus most of the extra charge on bcat is delocalized back to the Ru(acac)$_2$ fragment. The NPA analysis reveals the ionicity of the Zn complex (**8**) to a greater degree than the ECDA analysis since it indicates a charge on the metal approaching 2. The NPA charge on Fe reflects some covalency in the Fe acac bonding. We comment further on the oxidized and reduced bqdi species below.

Table 4 also contains a listing of the number of valence electrons (NPA) residing on Ru. This diminishes, with increasing π-back-donation, for Ru^{II}, from R = Me$_2$ (7.00 e) to NO$_2$ and *N*-Ms$_2$ (6.94 e). The value exceeds 6 because of σ-donation. It diminishes for the formally Ru^{III} species **1*a** and **7**, though by very little. The small change from the Ru^{II} species reflects a drastic reduction in π-back-donation as revealed by the increased positive charge on bqdi in **7**. Curiously, it increases in the Ru^{III} species **6** due to a much larger σ-donation from the formally dinegative ligand. The number of valency electrons on Ru is substantially larger

(80) Foster, J. P.; Weinhold, F. *J. Am. Chem. Soc.* **1980**, *102*, 7211–7218.
(81) Reed, A. E.; Curtiss, L. A.; Weinhold, F. *Chem. Rev.* **1988**, *88*, 899–926.

Table 4. Natural Population Analysis (NPA) of [Ru(acac)$_2$(R-bqdi)] and Related Species in Solution (PCM Acetonitrile Phase except Where Indicated (charge, a.u.))

#	R-bqdi complex	q(Ru)[a,b]	q(acac)[a]	q(R-bqdi)[a]	Q(N)(R-bqdi)[c]
1	Ru(acac)$_2$(H-bqdi)	0.98 (6.99)	−1.02	0.04	−0.61
1*a	[Ru(acac)$_2$(H-bqdi)]* S=1[d]	1.11 (6.86)[e]	−0.91	−0.20[f]	−0.66
2	Ru(acac)$_2$(Me$_2$-bqdi)	0.97 (7.00)	−1.04	0.07	−0.61
3	Ru(acac)$_2$(Cl-bqdi)	0.99 (6.98)	−0.99	−0.003	−0.60,−0.61
4	Ru(acac)$_2$(NO$_2$-bqdi)	1.03 (6.94)	−0.90	−0.13	−0.56,−0.62
5	Ru(acac)$_2$(*N*-Ms$_2$-bqdi) (C$_1$)	1.02 (6.94)	−0.74	−0.28	−0.58,−0.65
6	[Ru^{III}(acac)$_2$(H-bcat)]$^{-}$[g]	0.94 (7.03)	−1.27	−0.67[h]	−0.71
7	[Ru^{III}(acac)$_2$(H-bqdi)]$^{+}$ (g)	1.15 (6.82)[e]	−0.54	0.39[i]	−0.56
8	Zn(acac)$_2$(bqdi) (g)	1.73 (Zn) (10.25)	−1.77	0.04	−0.67
9	[Zn(acac)$_2$(bsqdi)]$^{-}$ (g)	1.73 (Zn) (10.25)	−1.83	−0.90[f]	−0.87
10	Fe(acac)$_2$(bqdi) (g)	0.92 (Fe) (7.04)	−1.03	0.11	−0.57
11	[Ru(bpy)$_2$(bqdi)]$^{2+}$ (g)	0.70 (7.26)	n.a.	0.27	−0.61
12	[Ru(mac(H$_2$O))(bqdi)]$^{2+}$ (g)	0.75 (7.22)	n.a.	+0.21	−0.64
13	[Ru(PPh$_3$)(CO)$_2$Br(bqdi)]$^{+}$ (xr)	−0.05 (8.03)	n.a.	0.36	−0.61

[a] Net charges on the moieties as indicated; (g) = gas phase, DFT optimized, calculation; (xr) X-ray structure was employed. [b] Natural population of valence orbitals (in electrons). [c] Net charge on each coordinating N atom. [d] Lowest excited spin triplet state of bqdi complex (geometry-optimized), formally Ru^{III}(acac)$_2$(H-bsqdi). [e] Sum of α and β electrons. [f] R-bsqdi. [g] See comments about the nature of this species containing Ru^{III} and the fully reduced diamidobenzene dianion (NH^{-}) in section 6.0. [h] Doubly reduced species. [i] ECDA calculation yields 0.31 e.

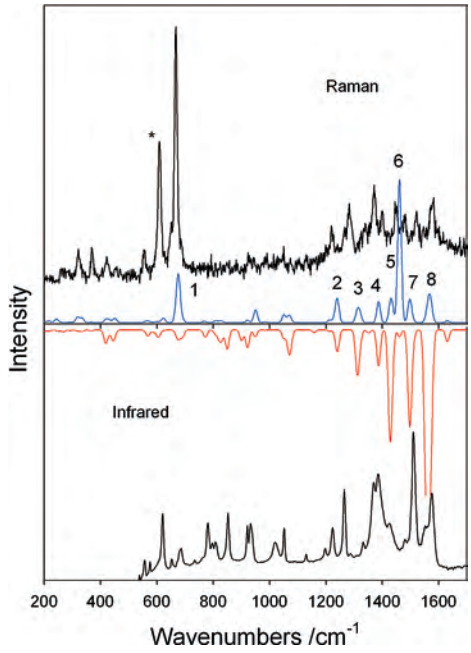

Figure 12. Infrared and resonance Raman (solid state sample) data for Ru(acac)$_2$(Cl-bqdi) (**3**). The upper panel shows the experimental (black, solid state) rR spectrum excited within the principal visible region absorption band and the DFT-calculated (not resonance-enhanced) Raman spectrum (blue). The asterisked peak near 600 cm^{-1} may arise from **3** situated in a secondary site in the crystal. The lower panel shows the experimental (black, neat sample) and the DFT (B3LYP/LANL2DZ) calculated (red) infrared spectra.

for species **11**−**13** which are expected to be much poorer π-electron donors to bqdi. The number of valence electrons in **8**, **9**, and **10**, lie in the ranges anticipated.

5. Vibrational and Electronic Spectra

5.1. Infrared and Resonance Raman spectra. There is generally excellent agreement between the Raman and infrared spectra of these species and the DFT-calculated data (see Figure 12 for the R = Cl species and for the infrared spectrum with R = Me$_2$ (infrared only)). We have previously reported and interpreted the resonance rR spectrum of the R = H species and also Ru(NH$_3$)$_2$Cl$_2$(bqdi) and Ru(2,2′-bpy)$_2$(4,5-Cl$_2$-bqdi) and a (O.O) quinone analogue [Ru(2,2′-bpy)$_2$(Q,O.O)]$^{2+}$, all with excitation via the intense visible region absorption (see Section 5.2).[50,60,82] The resonance enhancement provides evidence that the excited-state involved is localized mainly on the metallocycle ring.

The rR spectra of these aforementioned species are typified by an intense, resonantly enhanced, predominantly Ru−N(H) vibration ((Ru−O) for the quinone species) in the 500−650 cm^{-1} range together with, generally, only weakly enhanced vibrational features in the 1200−1700 cm^{-1} range associated with bipyridine and/or bqdi. The relative intensities provide evidence for the degree of distortion of the excited-state and all paint a picture where there is a major change in dimensions of the metallocycle ring but a much lesser effect on the quinonediimine phenylene ring. We provide additional evidence for this supposition, here for R = Cl (Figure 12). The experimentally observed, enhanced vibration at 667 cm^{-1} (calc. 677 cm^{-1}, vibration (1) in Figure 12) is mostly a symmetric Ru−N stretching vibration in the metallocycle ring causing a breathing motion weakly coupled to breathing of the benzoquinone ring. It is also coupled to the Ru−O(acac) symmetric stretching. The enhanced vibrations in the 1200−1600 cm^{-1} region comprise C=N vibrations of the bqdi metallocycle, various breathing vibrations of the acac and bqdi metallocycles, and rocking motion of the CH$_3$ groups of the acac rings. Details are provided in a footnote and further discussion is given below.[83]

5.2. Electronic Spectra. Ru^{II} R-bqdi complexes are formally expected to give rise to at least three low-energy metal metal-to-ligand charge transfer (MLCT) transitions: dπ→ bqdi π*, dδ→ bqdi π* and dσ→ bqdi π* (where bqdi π* is the LUMO of the complex, localized primarily on R-bqdi). The most intense of these transitions is always dπ→ π* due to the extensive mixing of the dπ and π* orbitals.

(82) Stufkens, D. J.; Snoeck, T. L.; Lever, A. B. P. *Inorg. Chem.* **1988**, *27*, 953–956.

(83) Raman footnote. 1. 677 cm^{-1} Symmetric Ru−NH stretching coupled with symmetric Ru−O stretching; 2. 1240.7 cm^{-1} Metallocycle NH wag; 3. 1312 cm^{-1} C−C acac; 1321 cm^{-1} bqdi C-H wag; 4. 1387 cm^{-1} C=N metallocycle symmetric stretch; 5. 1431 cm^{-1} CH$_3$(acac) wag; 6. 1461 cm^{-1} bqdi and metallocycle ring breathing mode, coupled to metallocycle NH wag; 7. 1496 cm^{-1} CH$_3$(acac) wag; 8. 1567 cm^{-1} bqdi and metallocycle ring breathing mode, coupled to metallocycle NH wag, and 1573 cm^{-1} acac ring breathing mode.

Table 5. TD-DFT-Calculated (TD-DFT) (more intense transitions only)[a] and Observed UV-Visible Spectral Data and Assignments for Ru(acac)$_2$(R-bqdi) Species

R [solvent]	observed transition υ /1000 cm^{-1} [ε /1000 M^{-1} cm^{-1}]	predicted transition[a] υ /1000 cm^{-1} (oscillator strength)	assignment[b]
H (**1**)	19.9 (13.8)	19.2 (0.23)	π-acac→ π*-bqdi, π-π*bqdi
[CH_3CN]		23.1 (0.06)	π-acac → π*-bqdi
	30.5 (5.3)	27.2 (0.06)	Ru d→ π*-acac
		28.7 (0.03)	Ru d, π-bqdi → π*-acac
	36.8 (16.9)	38.8 (0.09)	Ru d, π-acac → π*-bqdi
	42 sh	40.6 (0.16)	π-bqdi,Ru d, π acac → π*-acac
		43.0(0.22)	π-bqdi, π-acac → π*-bqdi
4,5-$(CH_3)_2$ (**2**)	19.5 (18.1)	19.4 (0.32)	π-acac→ π*-bqdi, π-π* bqdi
Me_2	29.9 (5.7)	23.7 (0.11)	π-acac → π*-bqdi, π-acac →d
[CH_3CN]		26.9(0.05)	d → π*-acac
		28.1 (0.04)	Ru, π-bqdi, π-acac → π*-acac
	36.8 (22.3)	38.7 (0.09)	Ru d → π*-bqdi
		40.5 (0.07)	π-bqdi, Ru d, π -acac → π*-acac
		40.6 (0.20)	π-bqdi, Ru d, π -acac → π*-acac
		41.9 (0.30)	π-acac, Ru d→ π*-bqdi
		50.1 (0.27)	π-acac → Ru d
		51.4 (0.69)	π-bqdi, π-acac → π*-bqdi
Cl (**3**)		18.6 (0.22)	π-bqdi, π-acac → π*-bqdi
[CH_3OH]	19.7 (22.2)	22.6 (0.11)	π-acac → π*-bqdi, π-acac → Ru d
		22.9 (0.06)	d-d
	30.3 (7.9)	27.8 (0.06)	π-π*-acac, Ru d → π*-acac
		37.6 (0.09)	Ru d, π-acac→ π*-bqdi
		38.9 (0.08)	π-bqdi, Ru d, πacac → π*-acac
	36.8 (26.4)	39.2 (0.08)	very mixed[c]
		40.6 (0.06)	Ru d, π-acac→ π*-bqdi
		40.8 (0.14)	π-bqdi, Ru d, πacac → π*-acac
		40.9 (0.13)	π-bqdi, Ru d, π-acac→ π*-bqdi
NO_2 (**4**)	18.9 (12.9)	15.4 (0.10)	π-bqdi, π-acac→ π*-bqdi
[CH_3CN]		17.4 (0.12)	π-bqdi, π-acac→ π*-bqdi
	21.0 (12.7)	21.2 (0.38)	π-acac→ Ru d, π*-bqdi
	23.9 (8.7)	24.5 (0.08)	π-bqdi, π-acac→ π*-bqdi
	30.9 (9.4)	29.0 (0.06)	π-bqdi, π-acac→ π*-bqdi
		29.5 (0.05)	Ru d, π-bqdi, πacac → π*-acac
		31.4 (0.07)	π-bqdi, Ru d, π-acac→ π*-bqdi
	37.3 (20.9)	39.6 (0.07)	π-bqdi, Ru d, πacac → π*-acac
		40.9 (0.07)	π-acac→ π*-bqdi
		42.0 (0.14)	π-acac→ π*-bqdi
		42.1 (0.07)	π-acac→ π*-bqdi
		42.2 (0.11)	very mixed[c]
	45.7 (17.0)	44.7 (0.06))	π-bqdi, Ru d, π-acac→ π*-bqdi
		47.9 (0.14)	π-acac → Ru d, π*-acac
(N-$SO_2CH_3)_2$ (**5**)	18.1 (6.2)	16.7 (0.07)	π-bqdi, π-acac→ π*-bqdi
Ms_2		18.0 (0.10)	π-acac→ π*-bqdi, π-acac→ Ru d
[CH_3CN]	21.3 (3.9)	20.9 (0.04)	π-bqdi, Ru d, π-acac→ π*-bqdi
		25.5(0.06)	π-bqdi, Ru d, π-acac→ π*-bqdi
	31.9 (7.5)	30.3 (0.05)	π-π* bqdi
	37.0 (14.1)	36.2 (0.06)	mixed[c]
		36.8 (0.05)	mixed[c]
		37.8 (0.05)	very mixed[c]
	41.0 (13.3)	39.0 (0.06)	very mixed[c]
		41.1 (0.06)	π-bqdi, π-acac→ π*-bqdi

[a] Only transitions with predicted oscillator strengths $f \geq 0.05$ are cited unless a weaker transition clearly relates to an observed feature. [b] Only the dominant contribution to the assigned transition is listed. [c] Many excitations with no clearly dominant one.

The dσ→ π* and dδ→ π* transitions are usually extremely weak because of poor overlap between ground and excited states. Magnuson and Taube[84] were probably the first to present this idea of the existence of both weak and strong charge transfer (CT) transitions in Ru π-acceptor ligand complexes.[53−57] Recent studies have shown that the separation between weak and strong CT transitions is dependent on the covalency of the bonds: a decrease in covalency is associated with a decrease in energy separation between the aforementioned strong and weak transitions such that, commonly, the latter are not observed because they are obscured by the strong transitions.[67] Our measurements revealed weak MLCT transitions with **1** (CH_3OH, 9000 cm^{-1}, ε 90 M^{-1} cm^{-1}), (also observed by Goswami et al.[23]) and with **2** (CH_3CN, 10000 cm^{-1}, ε 100 M^{-1} cm^{-1}). As we demonstrate below, however, the provenance of the most intense visible region transition, in these complexes, is not so straightforward as this treatment suggests.

The electronic transitions were derived using TD-DFT calculations (Table 5) using DFT-optimized structures and the PCM (acetonitrile). Most of the transitions do not exhibit any significant solvatochromism, with the exception of one of the transitions observed in the R = NO_2 species. The electronic absorption spectra are presented in Table 5, Figure

(84) Magnuson, R. H.; Taube, H. *J. Am. Chem. Soc.* **1975**, *97*, 5129–5136.

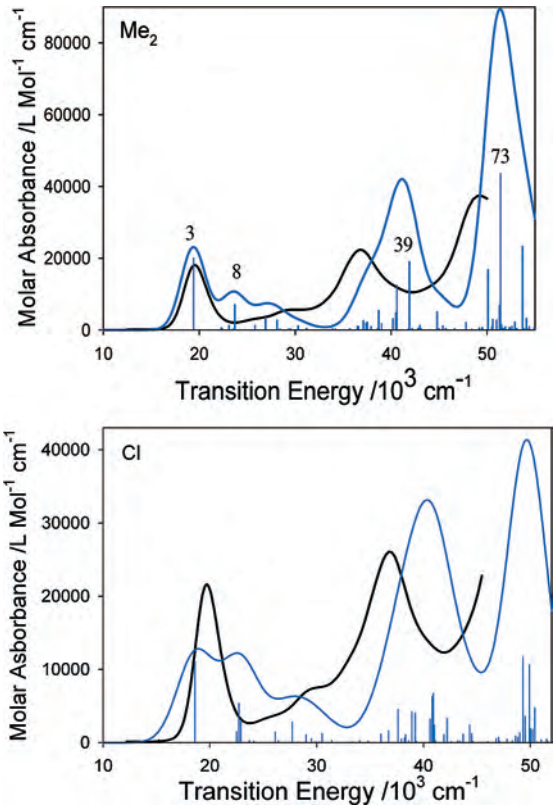

Figure 13. Experimental (black) and TD-DFT-predicted (blue, PCM) UV−visible absorbance spectra of (top) $Ru(acac)_2(Me_2\text{-bqdi})$ (**2**) (acetonitrile solution) and (bottom) of $Ru(acac)_2(Cl\text{-bqdi})$ (**3**) (methanol solution). Vertical bars indicate the locations of the predicted electronic transitions with relative oscillator strengths scaled to the molar absorbance. See Supporting Information Tables S5−9, Figure S-2 for further detail. More intense transitions, in the upper spectrum, are numbered sequentially from the lowest energy transition, according to Tables S5−9.

13 and in the Supporting Information Figure S-2. Generally, each observed band is an overlap of several discrete (calculated) transitions (Figure 13), and only the most intense transitions ($f \geq 0.05$) are discussed and tabulated here.

The complexes all display[85] the same general pattern of absorption, namely, three strong bands, one in the visible region centered near 20000 cm^{-1}, one between 35000−40000 cm^{-1} and a third transition above 40000 cm^{-1}. In addition it is evident that there are several weaker transitions between 20000 and 35000 cm^{-1} that appear as well-developed shoulders. The TD-DFT predicted transitions show exactly the same pattern generally with excellent agreement between the observed and predicted energy of the visible region band and reasonable agreement with the higher energy bands. The principle difference between the experimental and predicted spectra arises from the intensities of the predicted bands in the 20000−35000 cm^{-1} region being rather stronger than the experimentally observed ones; these intermediate bands are more clearly defined in the species (**4**) and (**5**). It is also evident from the predicted spectra that there are, in fact, a very large number of actual transitions lying under these "three" bands (Figure 13) such that a simple description of the provenance of these transitions is not straightforward.

However, some general assignments can be made. The intense visible region band (labeled 3 in Figure 13, R = Me_2 (labeling follows sequential listing of transitions in the Tables in Supporting Information)) is an excitation to the LUMO, dominantly from HOMO-2, but also partially from HOMO-3, all three of which involve the same dπ orbital. The provenance of the next predicted relatively intense transition, labeled band 8 in Figure 13, is then the reverse, dominantly from HOMO-3, with a smaller contribution from HOMO-2 → LUMO. Given the percentage makeup of the HOMO-2,3 and LUMO orbitals it is evident that these transitions can better be described by acac → bqdi ligand-to-ligand charge transfer (LLCT)[86] together with what is effectively an internal π-π* transition of the aromatic metallocycle; it is *not* then usefully described as Ru 4dπ →R-bqdi π* MLCT, although in some cases there is a small contribution from this, for example, where the d component of HOMO-2 exceeds slightly that of the LUMO. For example, for R = Me_2, transition 8 is primarily (Supporting Information, Table S-7): 65% HOMO-3 → LUMO, 7% HOMO → LUMO+3, 6% HOMO → LUMO+2. Then, reference to Table 2 reveals that this transition is mainly described as π-acac → π*-bqdi LLCT. Interestingly, there is also a π-acac to Ru d LMCT component to these transitions because the LUMO generally has more d character than HOMO-3 orbital.

The experimental evidence corroborating this conclusion arises from the rR data. In the previously analyzed resonance Raman spectrum with R = H, the most intensely enhanced band is the Ru−N stretching vibration at 646 cm^{-1}, while a somewhat weaker enhanced vibration appearing at 355 cm^{-1} is a coupled Ru−N, Ru−O motion.[16] There is also a set of weakly enhanced vibrations in the fingerprint region of which the two more intense experimentally observed vibrations occur at 1378 and 1400 cm^{-1}.[16] The former is mostly a symmetric C═N stretch in the metallocycle (coupled to CH motion of the bqdi ring) and the latter is an asymmetric C═O stretch in the acac metallocycle ring (coupled also to CH motion of the acac ligands). In the case of the R = Cl-bqdi rR spectrum (Figure 12, upper), the more intense vibration in the fingerprint region probably corresponds with the predicted band 4. This is mostly a C═N stretching vibration of the metallocycle which is *trans* to the chloride substituent, coupled to CH motion. Thus the rR data support the LLCT assignment. We note, in passing, a similar assignment for a strong visible absorption, dithiolate to diimine, in the spectrum of platinum diimine dithiolate species.[87]

For all R-bqdi, the less intense transitions near 30000 cm^{-1} can also be attributed to ligand-to-ligand charge-transfer (LLCT) absorptions and also MLCT, interestingly both d → π* bqdi *and* d → π* acac MLCT (see Table 5).[86,88] The principal absorption in the 35000−45000 cm^{-1} regime is

(85) Optical spectra for all of the complexes can be found in the Supporting Information section.

(86) Kunkely, H.; Vogler, A. *Eur. J. Inorg. Chem.* **1998**, *12*, 1863–1865.
(87) Cummings, S. D.; Eisenberg, R. *J. Am. Chem. Soc.* **1996**, *118*, 1949–1960.
(88) Benedix, R.; Hennig, H.; Kunkely, H.; Vogler, A. *Chem. Phy. Lett.* **1990**, *175*, 483–487.

clearly composite but the dominant component, for example, the transition at 43000 in H-bqdi is mostly HOMO-10 to LUMO which is a π-acac, bqdi $\rightarrow \pi^*$ bqdi transition. In R = Me_2, the strong band at 41,800 cm^{-1} (labeled 39 in Figure 13) is Ru 4d$\sigma \rightarrow \pi^*$ bqdi MLCT mixed with acac $\rightarrow$ bqdi LLCT. The very intense band (#73) near 50000 cm^{-1} seems to originate largely from acac to bqdi LLCT and internal π-π^* bqdi. See Supporting Information, Table S5−8, for further data especially for the lower symmetry R = Cl, NO_2 and for the more complex *N*-Ms_2 species. More detailed discussion of this last species will appear elsewhere.[77]

6. Ruthenium(II) or Ruthenium(III)?

We now turn to the question of whether these ruthenium species should be regarded as Ru^{II} derivatives of bqdi or spin-coupled Ru^{III} derivatives of bsqdi. There has been significant activity recently in trying to ascertain the charge or electron distribution in quinonoid systems, for example, see refs. 24, 25, 89−97. Indeed, as noted above, Wieghardt et al. specifically regard these acac/bqdi species to be best represented by $Ru^{III}(acac)_2$(bqsdi).[24] However, in an earlier paper, using the macrocycle 1,4,7-trimethyl-1,4,7-triazacyclononane, (mac), Wieghardt reported that [(mac)Ru-(H_2O)(bqdi)]$^{2+}$ definitively contained Ru^{II}, on the basis of the pK_a value for the coordinated water molecule.[98] These authors also remind us of the distinction, first made by Jørgensen, between formal oxidation states which are essentially physically meaningless, and spectroscopic oxidation states.[24,99] The former are derived automatically by heterolytically removing all the ligands with their closed-shell configuration; thus, in this case, the species are Ru^{II}-bqdi derivatives. The latter deals with the actual d^n configuration that is extant for the complex concerned and which must be based on experimental as well as theoretical considerations.

Traditionally, these species might be regarded simply as resonance hybrids of Ru^{II}-bqdi and Ru^{III}-bsqdi as noted by Remenyi and Kaupp.[25] Patra et al. came to a similar conclusion regarding (O,O) and (NH,O) quinone analogues bound to [Ru(acac)$_2$].[97] Remenyi and Kaupp note that calculations on the singlet state of species of this general class did not provide any convincing evidence for a broken-symmetry, open-shell state; this lack of a broken symmetry option, also implies a strong metal−ligand interaction which we know to be the case.[25,95] We now discuss arguments, which might favor one or other of these extreme viewpoints and develop a more succinct description of these species.

6.1. Synchrotron Data. Synchrotron Ru L-edge spectroscopy on several Ru(acac)$_2$(R-bqdi) species reveals the Ru L2 edge energy to be similar to those of $[Ru^{III}(NH_3)_5Cl]^{2+}$ and $Ru^{III}(acac)_3$, both of which contain Ru^{III}, and with an edge energy significantly more positive than that of, for example, $Ru^{II}(bpy)_2Cl_2$.[100]

6.2. NPA Interpretation. The natural population analysis data in Table 4 are very useful in assessing how these species should be regarded. That the NPA charge on R-bqdi is close to zero is itself an indicator that it should be regarded as a quinonediimine and not a semiquinonediiminate. Further, the semiquinonediiminate species [Zn(acac)$_2$(bsqdi)]$^-$ (Table 4) carries a significantly larger NPA negative charge than the parent bqdi species. The net negative NPA charge on the donor nitrogen atoms is significantly larger in bsqdi relative to bqdi. The NPA analysis of the oxidized species $[Ru^{III}(acac)_2(bqdi)]^+$ reveals a similarly small positive charge on R-bqdi and an NPA charge on the donor nitrogen equal to that of the parent Ru^{II} species. Thus, these NPA data point to the Ru^{II}-bqdi formulation. A more detailed discussion of the reduced and oxidized species will be published elsewhere.[77]

6.3. Bond Distances. A comparison of relevant bond distances shown in Table 6 is profitable. As noted by others[90,96,101] bond distances might be useful in determining the effective oxidation state of the ligand, and hence of the metal. Table 6 shows structural characteristics for some benzoquinonediimine and benzosemiquinonediiminate species and some standard values published initially by Pierpont with a more recent set from the Wieghardt group.[90,96] There is some disagreement between these two sets, but one conclusion seems to be unambiguous, namely, that the C−C bond alternation in the quinone oxidation state, with a shortest-longest C−C bond difference of 9−11 pm, is larger than that in the semiquinonate at 4−6 pm. A metallocycle C═N distance of ca. 130 pm is also a good marker for the quinone (135 pm for semiquinonate), but we will argue below that a C═N distance substantially longer than 130 pm does not rule out the quinone. In the discussion which follows, one must be cautious that bond distances derived from DFT may suffer some small error, and are probably too long.

There is surely no ambiguity over species **8**, **11** (**11a**) possessing M^{II} and benzoquinonediimine; similarly species **7**, with little back-donation from Ru^{III}, must contain bqdi and not bsqdi, despite the somewhat longer C═N distance. The iminoquinone analogue of **7** is also regarded as a Ru^{III}-quinone derivative.[97]

There would be no argument that species **1*a**, and **9** definitively contain bsqdi and we note the small alternating

(89) Chlopek, K.; Muresan, N.; Neese, F.; Wieghardt, K. *Chem. Eur. J.* **2007**, *13*, 8390–403.
(90) Ray, K.; Petrenko, T.; Wieghardt, K.; Neese, F. *J. Chem. Soc., Dalton Trans.* **2007**, 1552–1566.
(91) Blanchard, S.; Neese, F.; Bothe, E.; Bill, E.; Weyhermüller, T.; Wieghardt, K. *Inorg. Chem.* **2005**, *44*, 3636–3656.
(92) Herebian, D.; Bothe, E.; Neese, F.; Weyhermüller, T.; Wieghardt, K. *J. Am. Chem. Soc.* **2003**, *125*, 9116–9128.
(93) Kapre, R. R.; Bothe, E.; Weyhermüller, T.; DeBeer George, S.; Muresan, N.; Wieghardt, K. *Inorg. Chem.* **2007**, *46*, 7827–7839.
(94) Lu, C. C.; Bill, E.; Weyhermüller, T.; Bothe, E.; Wieghardt, K. *Inorg. Chem.* **2007**, *46*, 7880–7889.
(95) Kokatam, S.; Ray, K.; Pap, J.; Bill, E.; Geiger, W. E.; LeSuer, R. J.; Rieger, P. H.; Weyhermüller, T.; Neese, F.; Wieghardt, K. *Inorg. Chem.* **2007**, *46*, 1100–1111.
(96) Bhattacharya, S.; Gupta, P.; Basuli, F.; Pierpont, C. G. *Inorg. Chem.* **2002**, *41*, 5810–5816.
(97) Patra, S.; Sarkar, B.; Mobin, S. M.; Kaim, W.; Lahiri, G. K. *Inorg. Chem.* **2003**, *42*, 6469–6473.
(98) Juestel, T.; Bendix, J.; Metzler-Nolte, N.; Weyhermüller, T.; Nuber, B.; Wieghardt, K. *Inorg. Chem.* **1998**, *37*, 35–43.
(99) Jorgensen, C. K. *Coord. Chem. Rev.* **1966**, *1*, 164.
(100) Lever, A. B. P.; DeBeer George, S.; Solomon, E. I. To be submitted, 2008.
(101) Carugo, O.; Djinovi, K.; Rizzi, M.; Castellani, C. B. *J. Chem. Soc., Dalton Trans.* **1991**, 1551.

Table 6. Comparison of Key Bond Distances in Some Related Quinonediimine Species (pm)[a]

#	species[b]	M−N	C═N[c]	C1−C6[c]	C1...C5[d]
2	$Ru^{II}(acac)_2(Me_2\text{-bqdi})$ (s)	199	135	146	139, 146
1	$Ru^{II}(acac)_2$(bqdi) (s)	199	135	146	138, 144
1*a	$Ru^{III}(acac)_2$(bsqdi) S=1	200	137	145	140, 142
1b	**$Ru^{II}(acac)_2$(bqdi)** X-ray[e]	196	132	145	135, 144
6	$[Ru^{III}(acac)_2(bcat)]^{-}$[f]	202	137	146	141, 142
7	$[Ru^{III}(acac)_2(bqdi)]^{+}$	200	134	147	138, 145
8	$Zn(acac)_2$(bqdi)	224	130	152	137, 147
9	$[Zn(acac)_2(bsqdi)]^{-}$	214	134	149	139, 144
10	$Fe(acac)_2$(bqdi)	189	133	147	138, 145
11a	**$Ru^{II}(bpy)_2$(bqdi)** X-ray[g]	200, 203 (204)	130 (134)	143 (148)	136, 146 (138, 145)
12	$[Ru(mac(H_2O))(bqdi)]^{2+}$[h]	204	132	147	135, 144
13	$[Ru(PPh_3)(CO)_2Br(bqdi)]^{+}$	207	133	148	137, 146
14	$[Zn(acac)_2(bcat)]^{2-}$	205	138	148	140, 143
	bsqdi metric parameters[i]	n.a.	135	142 (143)[j]	137, 142 (136, 142)[j]
	bqdi metric parameters[i]	n.a.	130 (131)[j]	145 (148)[j]	134, 143 (134, 145)[j]

[a] Data are obtained from DFT B3LYP/LANL2DZ calculations except for species shown in bold that report X-ray data. [b] Gas-phase data are presented except where (s) denotes a PCM (acetonitrile) solution calculation results. [c] Within Ru metallocycle ring. [d] Minimum and maximum lengths of 'C−C═C−C═C−C' within quinonoid ring. [e] Ref. [f] bcat = dianionic benzoquinonediamido(2-). [g] From ref 52. Data shown in brackets are for DFT optimized structure (**11**). [h] Average X-ray determined distances for this complex where the water ligand was replaced with other monodentate ligands were[98] (in order of Table 6) 199, 132, 144, (135, 143). [i] From ref. [j] From ref.

Table 7. Bond Orders in the Metal-Quinonoid Fragment and Some of Its Reduced Analogues (DFT, B3LYP/LANL2DZ)[a] Listed in Decreasing Magnitude of Data in Column 3

complex	#	C3−C4, C5−C6[b]	C4−C5	C1−C2	C1−C6, C2−C3	C═N	M−N[b]
bqdi[c]		1.75	1.12	0.93	1.07	2.12	n.a.
$Zn(acac)_2$(bqdi)	**8**	1.75	1.11	1.00	1.08	1.72	0.20
$[Ru(PPh_3)(CO)_2Br(bqdi)]^{+}$	**13**	1.68	1.15	1.10	1.15	1.36	0.44
$[Ru(bpy)_2(bqdi)]^{2+}$	**11**	1.64	1.17	1.13	1.16	1.29	0.61
$[Ru(mac(H_2O))(bqdi)]^{2+}$[d]	**12**	1.64	1.17	1.14	1.17	1.30	0.62
$[Ru^{III}(acac)_2(bqdi)]^{+}$	**7**	1.64	1.18	1.12	1.18	1.24	0.68
$Ru(acac)_2(NO_2\text{-bqdi})$ (s)	**4**	1.63[e]	1.12	1.17	1.27	1.24	0.90
$Ru(acac)_2$(Cl-bqdi) (s)	**3**	1.60[f]	1.13	1.18	1.20	1.19	0.79
$Ru(acac)_2$(bqdi) (s)	**1**	1.60	1.22	1.17	1.21	1.20	0.78
bsqdi[c]		1.57	1.31	1.01	1.21	1.98	n.a.
$Ru(acac)_2(N\text{-}(SO_2Me)_2\text{-bqdi})$ (s)	**5**	1.57	1.24	1.19	1.23	1.05	0.68
$Zn(acac)_2$(bsqdi)	**9**	1.56	1.32	1.12	1.25	1.42	0.31
$Ru(acac)_2(Me_2\text{-bqdi})$ (s)	**2**	1.54	1.19	1.17	1.22	1.20	0.77
$Ru^{III}(acac)_2$(bsqdi) S=1	**1*a**	1.49	1.38	1.24	1.32	1.02	0.77
$[Ru^{III}(acac)_2(bcat)]^{-}$[g]	**6**	1.48	1.40	1.20	1.32	1.11	0.71
$[Zn(acac)_2(bcat)]^{2-}$[g]	**14**	1.37	1.51	1.18	1.41	1.21	0.46

[a] See Figure 1 for atom labels. DFT (Gaussian) optimized geometries in the gas phase, except where noted (s) (PCM, acetonitrile), derived using a normal population analysis and extracted with the AOMIX family of programmes.[39] [b] In asymmetric species, where the two bonds may have different bond orders, the higher value is quoted. [c] Free isolated ligand. [d] mac is 1,4,7-trimethyl-1,4,7-triazacyclononane. [e] Average of both bqdi ring C═C is 1.487. [f] Average of both bqdi ring C═C is 1.536. [g] bcat is the fully reduced (o-$(NH)_2C_6H_4$)(2-) species.

C−C difference. Species **6**, a one-electron reduced version of species **1**, has been previously described in related compounds as a Ru^{III} bound to the fully reduced dianionic ligand (equivalent to the catechol oxidation state) and lacks alternating C−C bond lengths except that the intrametallocycle C−C is longer.[25,98] Comparing the structural characteristics of these groups of complexes of well defined oxidation state, it is evident that the metric signature for bqdi is significantly different from that for bsqdi and bcat. The X-ray data for the R = H species (**1b**, Table 6) has structural characteristics which clearly lie inside the bqdi envelope and are not those of bsqdi or bcat, that is, formally to containing Ru^{II}. The Fe species also seems to be a Fe^{II} bqdi derivative. Species **8** and **11**, definitively bqdi, have the shortest C═N bond distance which is consistent with the quinonoid structure.

6.4. Bond Orders. Table 7 provides the NPA-derived bond orders derived from a natural population analysis. Obviously they reflect the bond distances shown in Table 6, but they do offer additional useful insight. We also include data for some asymmetric species which were not included in Table 6.

Table 7 includes data for the quinonoid oxidation level and for some one- and two-electron reduced derivatives. For reference purposes, we include data for the free ligands, bqdi and bsqdi, but note that their bond orders would be significantly affected by bonding to a metal center. The C1−C2 bond that conjoins the bqdi and metallocycle ring is always the weakest and longest bond in all three ligand oxidation states and does not vary very much. The internal bqdi ring C−C bond orders are most similar to each other in the fully reduced bcat species, less similar in bsqdi and vary most in the bqdi oxidation level, as we anticipate, and thereby provide a parallel view to the bond distances. On this basis, the one-electron reduction product species **6** clearly adheres to the Ru^{III}-bcat description.

To return to the problem of identifying species **1**−**5**, we can define species **8** (top of Table 7) unequivocally to contain

bqdi and it has the largest bqdi C═C bond order. Dicarbonyl species **13** as a dicarbonyl surely also contains Ru^{II} and bqdi, and has the second largest C═C bond order of the complexes in this tabulation. Similarly, the third- and fourth-largest, species **11** and **12**, surely also contain Ru^{II} and bqdi, based on the stabilization effect of bipyridine in the former and the recorded pK_a for coordinated water in the latter.[98] We have argued that species **7** must also contain bqdi, and its ring bond orders are essentially the same as the previous species, aside from a somewhat smaller C2−C3 value. We now arrive at species **1**−**5** and it would be difficult to argue that species **1**−**5** are dramatically different from those top 5 species. Thus the bond order values for species **4** and **7** are essentially indistinguishable. We then note that the sequence of bond orders (in column 3) for species **1**−**4** is actually inverted, relative to the degree of π-back-donation, that is, species **4** with the most π-back-donation (and most net negative charge) has the highest bond order. This is a counterintuitive result, albeit we list the higher bond order component of the two C═C bond orders in the asymmetric species **3** and **4**. Indeed, it is difficult to make an appropriate comparison with the asymmetric species where the chloro and especially the nitro substituents have a strong influence on the ring bond orders. However, the average of the C═C−C═C is 1.5 (1.6 for R = H). The orders of the other bonds in the quinone ring are also essentially the same as each other, showing for species **1**−**4** that although there is increasing back-donation, for example, as seen by the steadily increasing bond order of the Ru−N bond, the extra charge has little effect on the quinone ring.

The C═N bond order is 1.2 for species **1**−**4**, the same as for species **7** and only 0.1 below that, 1.3, for the other, indisputably, bqdi species (**11**, **12**). This value is substantially below the C═N bond order for Zn species **8** for reasons we now develop. Species **5** is a special case because the C═N group is conjugated directly to the methanesulfonyl substituents.

6.5. Electron Delocalization in the Metallocycle Ring. In the Ru^{III}-bsqdi limiting model, the coupled spin singlet pair of electrons on Ru^{III} and bsqdi would be HOMO-2. The corresponding spin triplet (Franck−Condon state, CH_3CN solvent) is calculated to lie at ca. 3780 cm^{-1} for S = 1 Ru(acac)$_2$(bqdi) (**1**) a very large singlet−triplet separation. However, this is not the lowest lowest-lying spin triplet; the triplet associated with the HOMO → LUMO transition which uncouples the dδ electrons is predicted to lie at 1220 cm^{-1}. The pair of electrons in the coupled Ru^{III}-bsqdi bond (HOMO-2) would formally be 50:50 evenly shared between the two components such that, averaged over time, the bqdi would have one extra electron in its π* LUMO, that is, it would be a semiquinonediiminate. In fact, one may calculate (ECDA, PCM) that HOMO-2 (in species **12**) is comprised of 61.8% HOF_1O of fragment 1 [Ru(acac)$_2$] and 26.2% of the LUF_2O of bqdi plus small contributions from other MOs of fragments 1 and 2, far from the 50:50 even split.

In the Ru^{II}-bqdi limiting model, HOMO-2 is responsible for most of the π-back-donation. Figure 14 shows the HOMO-2 for bqdi and reveals how it is constructed. One

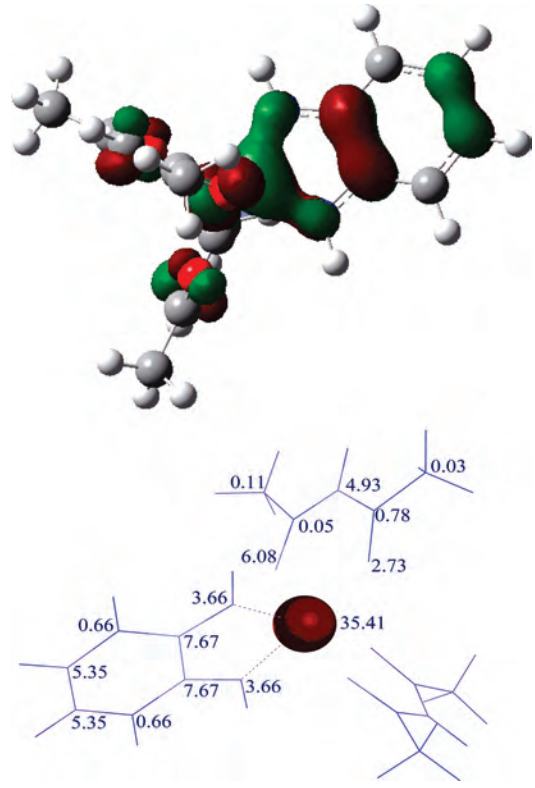

Figure 14. (Upper) The HOMO-2 of Ru(acac)$_2$(bqdi) (**1**) B3LYP/LANL2DZ, PCM (Lower) Percent contributions of individual atomic orbitals of Ru(acac)$_2$(bqdi) **1** to HOMO-2. The percent contributions in the lower acac ring are the same as in the upper acac ring. H-atom orbital contributions are essentially zero and are not provided.

can clearly see that the Ru−N,N side of the metallocycle ring comprises a 3-center, 2-electron π-bond which, in association with the 2 C═N π-bonds, explains the *pseudo*aromatic 6-electron behavior of this ring.[15−17]

Further, it is evident that relatively little (some 11%) of HOMO-2 resides on the C═C double bonds of the benzoquinone ring. Thus, the pair of electrons in this orbital is dominantly localized on the [Ru(acac)$_2$] and Ru-NH and C−C metallocycle fragments, thereby, explaining why the geometry of the benzoquinone ring, and the bond orders therein, are not significantly affected by increasing π-back-donation. Note also that HOMO-2 is antibonding with respect to the metallocycle C═N bonds, explaining why the C═N bond distance in these species is longer (and bond order smaller) when π-back-donation is significant; it is also antibonding with respect to the Ru−O(acac) bonds. Importantly, this view is corroborated by the resonance enhancement of the Ru−N, C═N and Ru−O stretching vibrations when excited in the principal visible-region absorption band, arising from excitation out of HOMO-2.

For completion we comment on an alternate model of the Ru^{III}-bsqdi species, namely as a broken symmetry antiferromagnetically coupled singlet (diradical), with one 4d(t_{2g}) electron and one electron in the π*-LUMO. This possibility had been eliminated by Remenyi and Kaupp,[25] and our calculations show that this is an excited-state relative to the Ru^{II}(bqdi) ground state, albeit a singlet diradical has been proposed for a ruthenium complex of a phenylazopyridine ligand.[102]

Overall, then, we conclude that the best representation of these species is indeed as Ru^{II} complexes of substituted benzoquinonediimines exhibiting extensive π-back-donation into the metallocycle ring, rather than as Ru^{III} complexes of benzosemiquinonediiminates. This analysis confirms the unusual character of the noninnocent bqdi ligand capable of responding in quite a dramatic fashion to the changing acceptor and donor characteristics of the metal to which it is bound, such characteristics being readily modifiable through change of other coligands (often called spectator ligands but here they are hardly just spectating!). The synchrotron data noted above then reflects the extra positive charge residing in the ruthenium Ru atom due to extensive π-back-donation and not that these species must be regarded as Ru^{III}.[100] A key observable, illustrative of the variation of net charge residing on the R-bqdi ligand, is the electrochemical reduction potential, of bound bqdi to bound bsqdi, which varies over an astonishingly large range.[103]

Acknowledgment. A.B.P.L. and P.G.P. are indebted to the Natural Sciences and Engineering Council (NSERC, Ottawa) for financial support. C.D. also thanks NSERC for a postgraduate scholarship. We also thank the Johnson-Matthey Company for the loan of ruthenium chloride, and Gwenaël Malbec and Prof. Christian Reber (Université de Montreal) for the resonance Raman data. This work was made possible by the facilities of the Shared Hierarchical Academic Research Computing Network (SHARCNET: www.sharcnet.ca).

Supporting Information Available: Tables of selected bond distances, NMR chemical shifts, predicted optical spectra and assignments, selected molecular orbital compositions and orbital interaction diagrams, *xyz* atomic coordinates and electrochemical data, are provided. Complete ref. 30 is provided. This material is available free of charge via the Internet at http://pubs.acs.org.

IC8014496

(102) Samanta, S.; Singh, P.; Fiedler, J.; Záliš, S.; Kaim, K.; Goswami, S. *Inorg. Chem.* **2008**, *47*, 1625–1633.

(103) Lever, A. B. P., 2008, in preparation.